

PRAOMS: Entwicklung eines prä-operationellen Assimilationssystems für Ozean- und Meereisfelder aus Satellitendaten

[07 DLR 09 D11]

Abschlussbericht

Ulrich Cubasch und Detlev Müller

Max-Planck-Institut für Meteorologie. Hamburg

1 Project objective

The comprehensive study of climate variability and change requires the availability of homogeneous, global data sets. For the documentation of climate fluctuations, WRCP/WMO projects currently assemble a corresponding data library for the atmosphere (GCOS) and for the ocean (GOOS). On this background, the scientific and research political objectives of PRAOMS are:

Development a pre-operational system for the collection of satellite data of the global ocean and their assimilation into a state-of-the-art ocean circulation model (Figure 1).

Assemble a library of global, homogeneous and consistent ocean data (e.g. sea-surface temperatures (SST), sea-ice coverage, ocean currents, sea-level (SSH), heat fluxes).

This library should provide a data basis for monitoring and analysing climate fluctuations and contribute to the goals of GCOS and GOOS. Moreover, these data apply as input to seasonal predictions.

As an option, the system's regional skill in the European seas should be tested.

After conclusion of the development phase, the system should be fitted in a separate project (e.g. the pilot-SAFs "Climate Monitoring" (DWD) or the Meteo-France SAF "Ocean and Sea Ice") to then operational satellite missions. It was planned, in particular, to transfer the system to EUMETSAT or to the DWD for routine operation as ground segment in EUMETSAT satellite missions.

The main objective of PRAOMS is the prevention of an essentially unused archiving of novel satellite data (namely those of EUMETSAT). The PRAOMS data processing system makes this information accessible to various counselling- and science-centres, providing a hierarchy of products ranging from raw satellite data to global ocean state estimates.

In this joint project, MPIMET developed an assimilation system on the basis of existing ocean circulation models and assimilation software. System development took several stages due to restrictions in the available computing resources:

The Hamburg LSG Model was used as a preliminary numerical ocean circulation model. The model, already used for assimilation purposes in the German WOCE project, has a horizontal

UNIVERSITÄTSBIBLIOTHEK
HANNOVER
TECHNISCHE
INFORMATIONSBIBLIOTHEK

1

06.09.2002

UB/TIB Hannover 89
121 047 547



resolution of 3.5° and 11 layers in the vertical. In the present framework, it is used for the Adjoint assimilation of buoyancy data.

Secondly, the GROB HOPE model with a resolution of 3° and 20 levels in the vertical was applied in Sequential Assimilation (Kalman-filter).

Thirdly, an Adjoint version of the C-HOPE model with a horizontal resolution of 2° (and equatorial refinement to 0.5°) and 20 layers in the vertical has been developed. However, at the end of the project it was still in its testing phase and it has not yet been used to assimilate data.

The paper is organized as follows: Section 2 introduces the analysed data sets. Section 3 describes the numerical ocean circulation models while Section 4 discusses the two assimilation techniques and their implementation. Results from these different set-ups are shown in Section 5, followed by a Summary (Section 6) and outlook (Section 7).

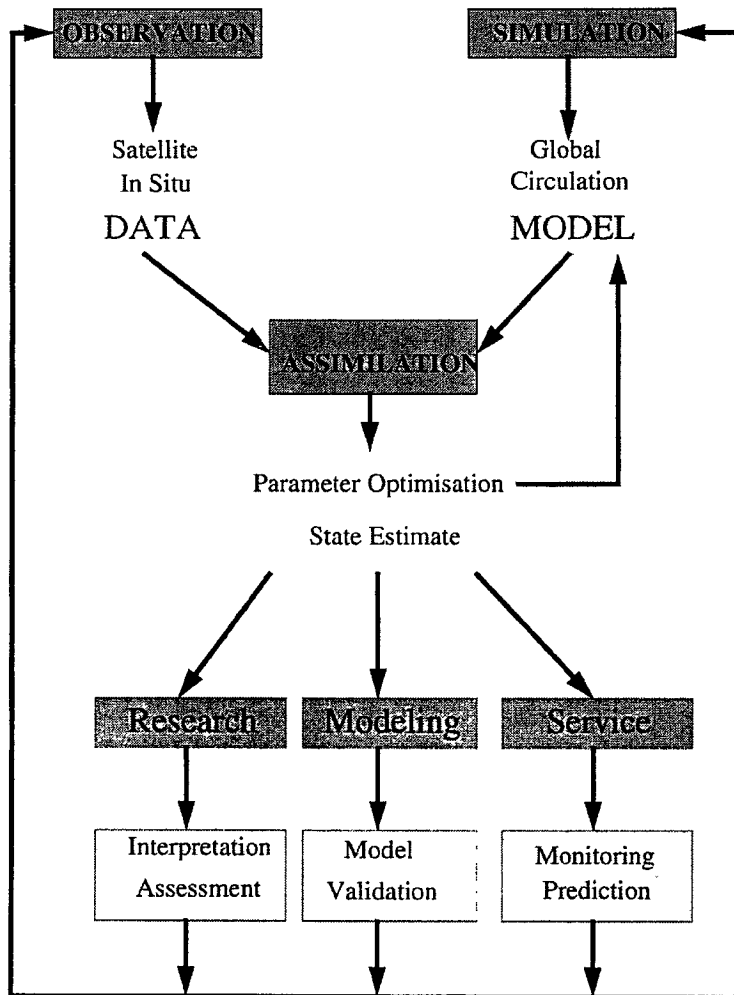


Figure 1: Schematic diagram of a quasi-operational data assimilation system.

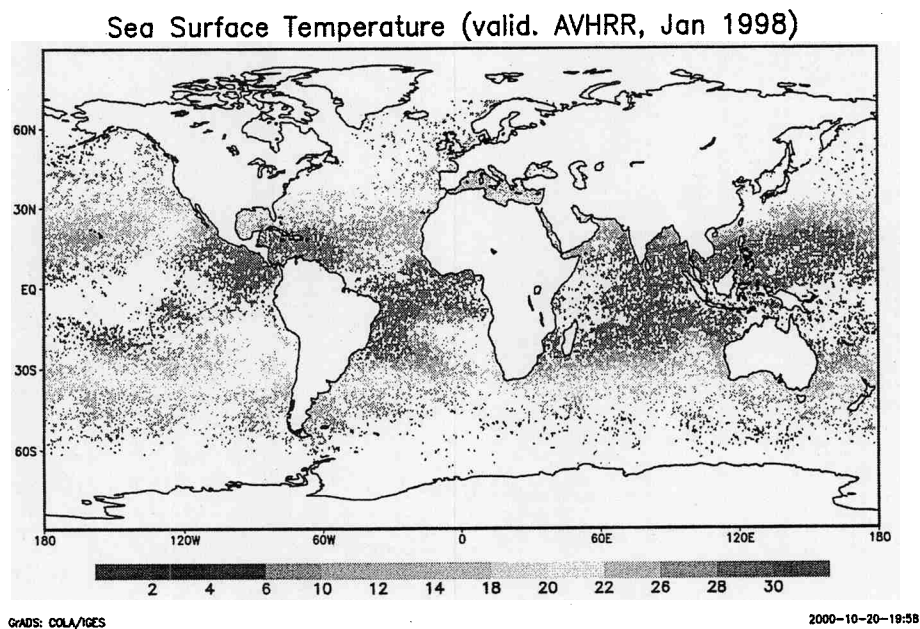
2 Datasets

2.1 Satellite Data Sets

Sea surface temperatures: NOAA AVHRR:

The NOAA/NASA AVHRR Oceans Pathfinder sea surface temperature data are derived from the 5-channel Advanced Very High Resolution Radiometers (AVHRR) on board the NOAA-7, -9, -11 and -14 polar orbiting satellites. The data set of sea surface temperatures with a sufficient spatial and temporal coverage is available from the Jet Propulsion Laboratory ([ftp: po-daac.jpl.nasa.gov](ftp://po-daac.jpl.nasa.gov)). The global data set begins in November 1981 with a spatial resolution of 18 km. The calculation of the weekly and monthly mean is based on the Multi-Channel SST (MCSST) algorithm. Sea surfaces temperatures are estimated with MCSST from the two thermal channels 4 and 5 by applying the split window technique (McClain et al., 1985). This method uses the advantage that channel 5 recognizes a higher extinction than channel 4 because of a higher absorption of water vapour molecules. The measured emission can be described as a superposition of the emission of the Earth's surface and the atmosphere. Therefore, the sensor detects lower emission for channel 5 over the ocean. Considering a known emission of water in the thermal spectrum, differences between radiative temperatures can be used to estimate the sea surface temperature. This so-called skin temperature is generally about 0.1°C to 0.5°C lower than the temperature of the surface water masses, which is also named bulk temperature. Monthly mean values of surface temperatures have been interpolated spatially (Figure 2) and to the model grid (Figure 3).

(a)



(b)

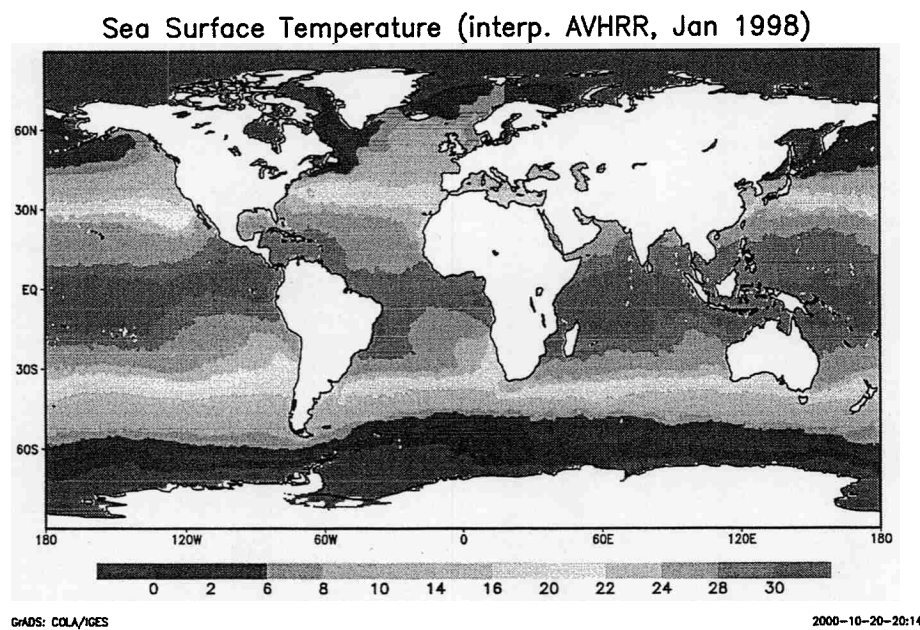


Figure 2: Sea surface temperature (January 1998) derived from the AVHRR sensor on the NOAA satellite with MCSST algorithm. (a) raw data, and (b) globally interpolated data.

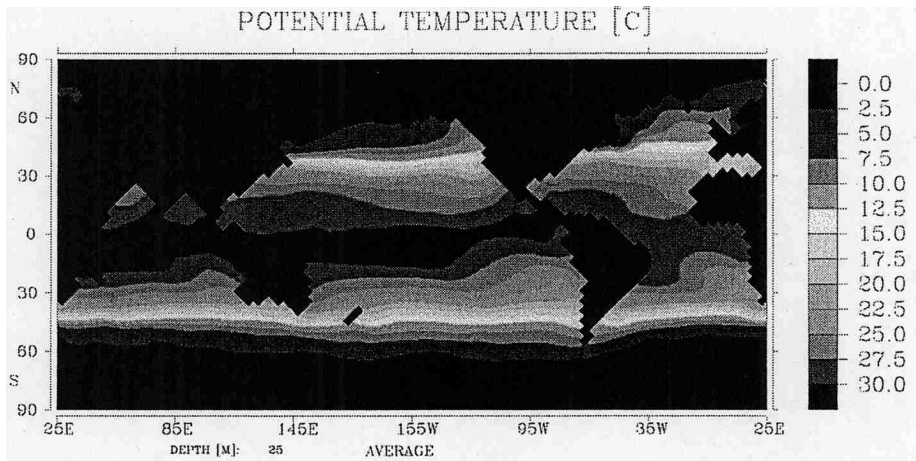


Figure 3: Sea surface temperature from Figure 1 interpolated to the model grid of a large-scale ocean general circulation model.

2.2 Reanalysis Data Sets

Sea surface temperatures and wind stress: ECMWF Reanalysis Data:

Operational analyses are affected by major changes in models, analysis technique, assimilation, and observation usage, which are an essential product of research and progress. The ECMWF (European Centre for Medium-Range Weather Forecasts) performed a consistent reanalysis of atmospheric data using a "frozen" production system. The ECMWF Re-Analysis (ERA) Project produced a new, validated 15-year data set of assimilated data for the period 12/1978-02/1994. The assimilation scheme consisted mainly of the Integrated Forecast System (IFS) version of the ECMWF forecast model with T106 resolution on 31 vertical hybrid levels. An intermittent statistical (optimum interpolation) analysis with 6-hour cycling was performed. It includes a diabatic, non-linear normal mode initialisation (5 vertical modes). The data sets (T106 resolution) consist of monthly means of 24h-forecast surface fields. Data are available from the CERA data server at the German Climate Computing Centre DKRZ. Monthly mean values of air surface temperatures and wind stress have been calculated and interpolated to the model grid. The climatologically monthly means of these data have been taken as prescribed surface boundary condition to generate the model climatology hereafter named reference run.

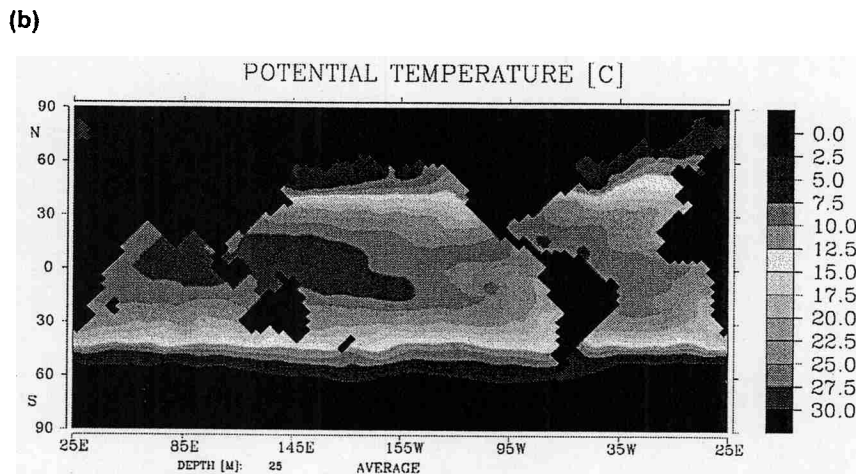
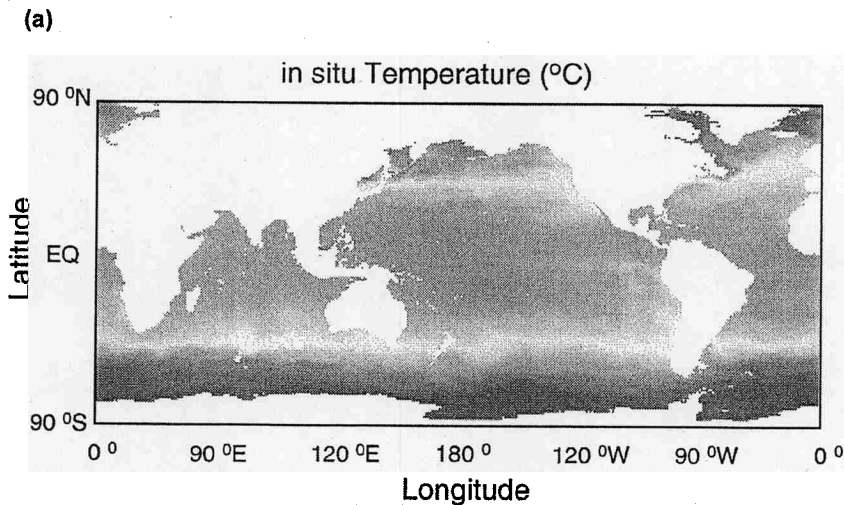


Figure 4: (a) Annual mean climatology of sea surface temperature of marine in situ observations from WOCE special analysis centre (SAC). Temperature ranges from -1.8°C (dark blue) to 29.5°C (red). (b) Data interpolated to the model grid of a large-scale ocean general circulation model.

2.3 Hydrographic Data Sets

Temperature, Salinity, and Oxygen: WHP Special Analysis Center:

The World Ocean Circulation Experiment (WOCE) Hydrographic Program (WHP) Special Analysis Center in Hamburg has prepared a climatology for the world ocean with objectively analysed mean fields of temperature, salinity and oxygen (Gouretski and Jancke, 1998). Data base, quality control procedure, optimal interpolation method, vertical and horizontal resolution of this climatology differ from the previous World Ocean climatology produced by the NODC Ocean Climate Laboratory (Levitus et al., 1994; Levitus, 1994). Important differences between the World Ocean Atlas 1994 and the climatology used here include

a more elaborate quality control method resulting in a more reliable identification of erroneous and untypical data;
an optimal interpolation on neutral surfaces, thus avoiding production of artificial water masses
a better vertical resolution.

No information from data close to the bottom is lost. Further, more high-quality data (both WOCE and non-WOCE) were added to the NODC data set to substantially improve data coverage in areas of sparse data and in the deepest layers. Also, a more accurate representation of the deep-water patterns and of the temperature/parameter relationships is achieved.

The annual mean climatological database has been interpolated to the model grid (Figure 4). Future work will include a seasonal cycle and consideration of WOCE single profiles (Gouretski, pers. com.).

3 The ocean models

3.1 The Large-scale geostrophic (LSG) ocean model

A description of the current version of the Hamburg large-scale geostrophic OGCM (LSG) (Maier-Reimer et al., 1993) is given by Winguth et al. (1999). The Hamburg LSG uses a 72 x 72 E-grid (Arakawa and Lamb, 1977) (approximately $3.5^{\circ} \times 3.5^{\circ}$ horizontal resolution), 11 vertical layers, and has a time step of one month. The temperature and salinity in the surface layer were computed by a Newtonian coupling to prescribed ECMWF Reanalysis air temperatures (Section 2.2) and surface salinities of Levitus et al. (1982). The sea ice model is a simple thermodynamic model including a wind-dependent ice advection. Further details are found in Mikolajewicz (1996) and Winguth et al. (2002). Coupling coefficients of $40 \text{ W m}^{-2} \text{ K}^{-1}$ for temperature and $1.5 \times 10^{-5} \text{ m s}^{-1}$ for salinity yield with a 50-m thick top layer) time constants for both properties of approximately 60 and 40 days, respectively.

3.2 The Hamburg Ocean Primitive Equation Model HOPE-C

During the course of the project, a new model version of the Hamburg Ocean Primitive Equation Model (HOPE) model became available. Its earlier versions had been tested in many sensitivity studies of the ocean-atmosphere system (Drijfhout et al., 1996; Stoessel et al., 1998) and its coupling to the atmosphere (Latif et al., 1994; Latif and Barnett, 1996; Stockdale et al., 1994; Groetzner et al., 1998; Legutke and Voss, 1999; Venzke et al., 2000).

The quantitative estimates of the sensitivity require a mathematical model of the phenomena or relationship. The studies above have used the HOPE to determine impacts of the perturbations and thereby to estimate the sensitivity. A more efficient, revealing and direct way is to use the model's adjoint (e.g. Tziperman et al., 1992; Giering, 1996; Winguth, 1997; van Oldenburgh et al., 1997; Müller et al., 1998; Marotzke et al., 1999; Giering, 2000; Winguth et al., 2000; Stammer et al., 2000; Wenzel et al., 2001).

C-HOPE, the Arakawa C-grid version of HOPE, is an improved version of the HOPE-E documented by Wolff et al. (1997) and HOPE-G (Legutke and Maier-Reimer, 1999). A de-

tailed description of C-HOPE can be also found in Marsland et al. (2002). It is a global Primitive Equation model of the general ocean circulation using depths as vertical coordinate (Figure 5). It contains a free surface and a dynamic-thermodynamic sea ice model with viscous-plastic rheology and snow. C-HOPE uses a horizontal curvilinear grid (conformal mapping of geographical coordinates, Figure 6) to accommodate increased resolution in regions of interest without the interior boundary problems of nested models. The standard grid set-up used for climate studies has a horizontal spatial resolution ranging from 8 km to 250 km. The North Pole is placed in Greenland to avoid distorted physics in the Arctic Ocean, as shown below in Figure 6. The South Pole, while remaining over land, is moved to an equivalent distance along the same longitude line to keep the zero-latitude line along the equator. The standard grid set-up also contains enhanced meridional resolution in the tropics. The vertical resolution is 23 levels with increasing thicknesses.

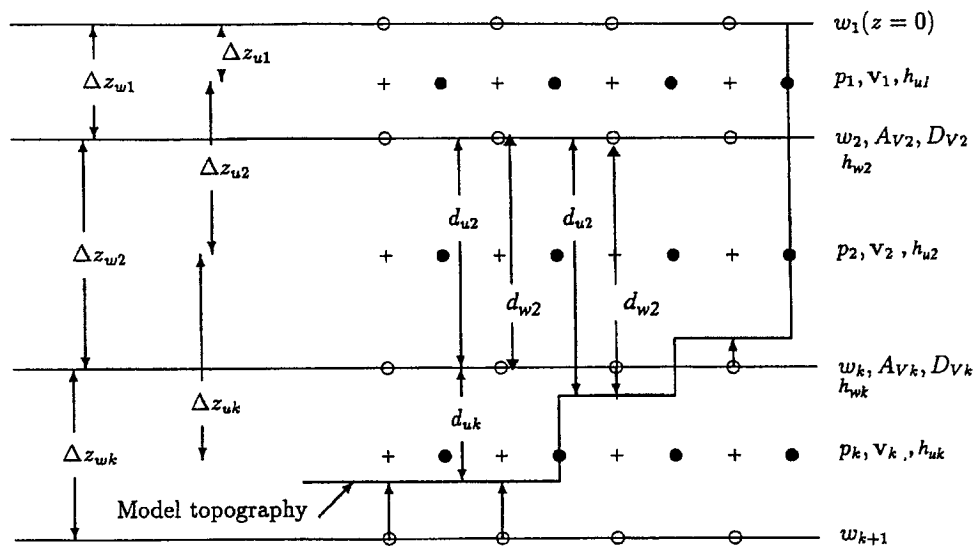


Figure 5: Configuration of the vertical model grid. The thickness of the layers increases with depth from 20 m at the surface to 1400 m in the bottom layer. The thickness of the lowest box in each column is adapted to the local bathymetry. Filled circles denote location of horizontal vectors (e.g. velocities). Vertical velocities (open circles) are calculated at points that are shifted horizontally and vertically relative to the location of horizontal velocities on the grid.

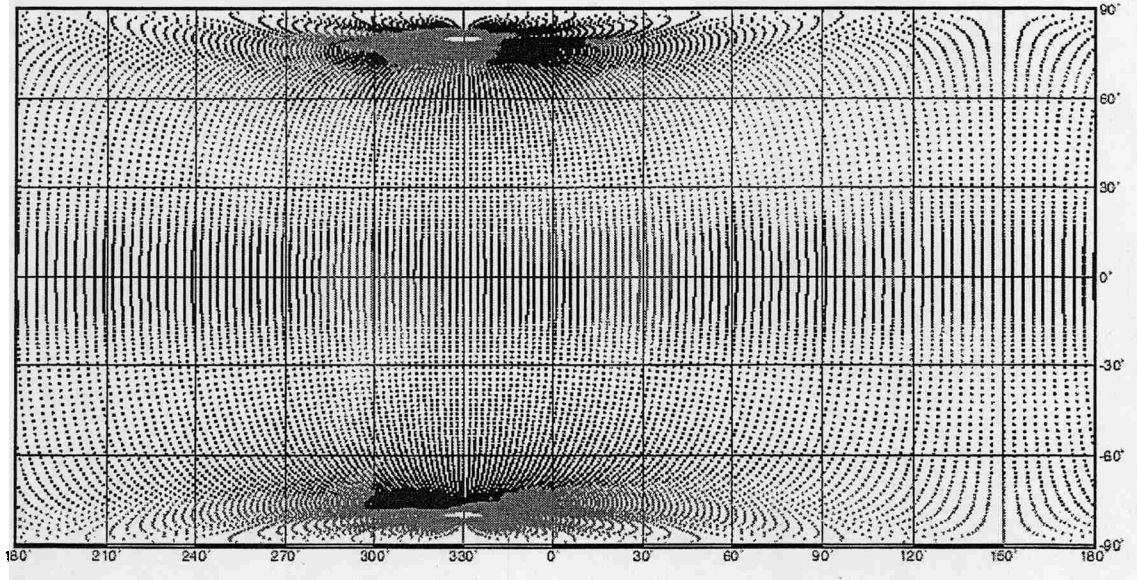


Figure 6: Configuration of the horizontal model grid.

3.2.1 Model Physics

The model is based on the non-linear balance equation for momentum, the continuity equation and conservation equations for heat and salt for an incompressible, hydrostatic Boussinesq-fluid on a rotating sphere. Prognostic variables of C-HOPE are horizontal velocities \bar{v} , potential temperature θ and salinity S , and sea-surface elevation ζ . The internal pressure $p = g \int_0^z \rho dz$ is calculated by using the hydrostatic equation with a non-linear polynomial equation of state (Fofonoff and Millard Jr., 1983). The horizontal momentum equation is given by

$$\frac{d\bar{v}}{dt} + f(\bar{k} \times \bar{v}) = -\frac{1}{\rho_0}(\bar{\nabla}_H(p + \rho_0 g \zeta)) + \bar{F}_H + \bar{F}_V \quad (1)$$

where \bar{v} is the horizontal velocity vector, f the Coriolis parameter, \bar{k} the upward vertical unit vector, ρ_0 the constant reference density, g the gravitational acceleration on earth. The friction terms \bar{F}_H and \bar{F}_V are parameterisations of the horizontal and vertical eddy viscosity, respectively.

The vertical velocity is calculated diagnostically from the incompressibility condition

$$\frac{\partial w}{\partial z} = \bar{\nabla}_H \bar{v} \quad (2)$$

The sea surface elevation is calculated from the internal linearized kinematic boundary condition:

$$\frac{\partial \zeta}{\partial t} = w|_{z=0} + Q_z \quad (3)$$

The kinematic boundary condition at the surface is specified by

$$\tau = \rho_0 A_v \frac{\partial \vec{v}}{\partial z} \Big|_{z=0} \quad (4)$$

The conservation equations for potential temperature θ and salinity S are given by

$$\frac{d\Theta}{dt} = K_H \bar{\nabla}_H \Theta + \frac{\partial}{\partial z} K_V \frac{\partial \Theta}{\partial z} \quad (5)$$

$$\frac{dS}{dt} = K_H \bar{\nabla}_H S + \frac{\partial}{\partial z} K_V \frac{\partial S}{\partial z} \quad (6)$$

The horizontal eddy diffusivity coefficient K_H is grid-size dependent with a value of $K_H=1.0 \cdot 10^3 \text{ m}^2 \text{ s}^{-1}$ at 400 km grid distance. The current version of C-HOPE includes isopycnal diffusion and a Gent-McWilliams type eddy parameterisation (Gent and McWilliams, 1990) to improve the mixing along isopycnals observed from tracer distributions.

The vertical eddy diffusivity depends on the local Richardson number and additional wind mixing. In case of unstable density stratification, increased vertical diffusivity adjusts the density of the water column until it reaches a neutral or stable stratification. The current version includes a bottom boundary layer slope convection scheme for a better representation of the flow of relatively dense water over sills and at the continental slope.

Sea ice motion is determined by a two-dimensional momentum balance equation

$$\frac{\partial \vec{v}_i}{\partial t} + \mathbf{f}(\vec{k} \times \vec{v}_i) = -g \bar{\nabla}_H \zeta + \frac{\vec{\tau}_a}{h_i \rho_a} + \frac{\vec{\tau}_o}{h_i \rho_i} + \bar{\nabla}_H \cdot \sigma_{mn} \quad (7)$$

The ice motion with sea ice thickness h_i and density of the ice ρ_i responds to wind stress $\vec{\tau}_a$ and ocean current stress $\vec{\tau}_o$, and internal ice stress represented by the two-dimensional stress tensor σ_{mn} for sea ice rheology according to Hibler (1979).

The flow chart of the models time loop is shown in Figure 7. For a detailed description of the subroutines, we refer to Wolff et al. (1997) and Marsland et al. (2002).

3.2.2 Surface Boundary Condition for Heat

The net surface heat flux from the atmosphere Q_a is balanced by the net surface flux from the ocean Q_o or from sea ice Q_i with a fractional sea ice coverage A per grid cell:

$$Q_a = (1 - A)Q_o + AQ_i \quad (8)$$

with

$$Q_m = (1 - \alpha_m)Q_m^{sw} + Q_m^{lw \downarrow} + Q_m^{lw \uparrow} + Q_m^{la} + Q_m^{se} ; m = o, i$$

Q_m^{sw} denotes the incident short-wave radiation reduced by the albedo (reflectivity) of the surface, $Q_m^{lw \downarrow}$ downward long-wave radiation, $Q_m^{lw \uparrow}$ the upward long-wave radiation proportional to the 4-th power of the surface temperature, Q_m^{la} the latent heat flux which is proportional to the evaporation, and Q_m^{se} the sensible heat flux which is proportional to the temperature gradient between the surface and the air in the surface boundary layer.

FLOW CHART OF OCEAN MODEL C-HOPE (FORWARD MODEL)

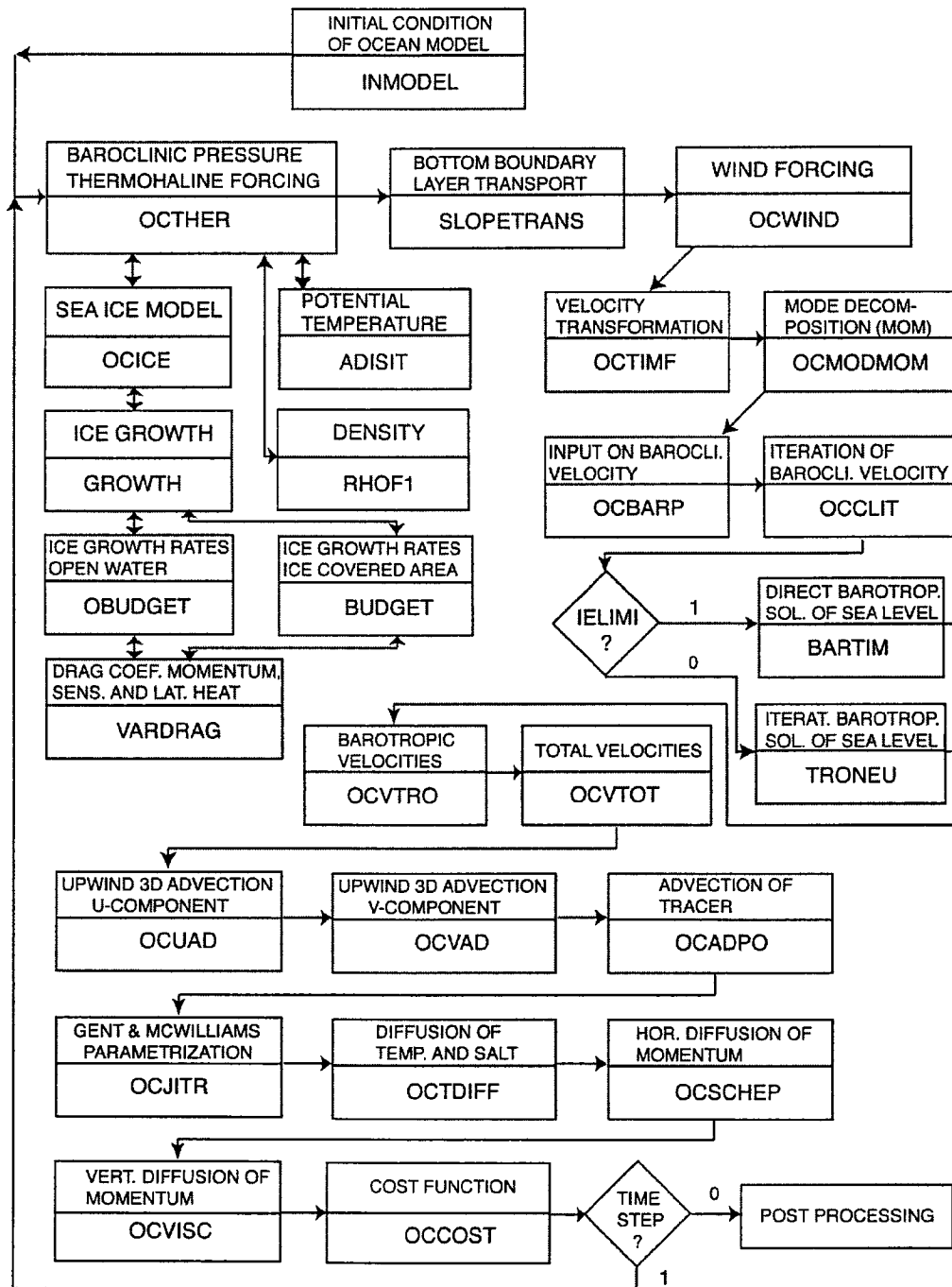


Figure 7. Flow Chart of the C-HOPE time loop.

3.3 The Hamburg Ocean Primitive Equation Coarse resolution Model GROB HOPE

The present study utilizes GROB HOPE, a coarse version of the HOPE-C model. It has 20 layers in the vertical with high resolution of 10 layers in the upper 500m. In the horizontal, the model uses a spatially inhomogeneous grid obtained from a conformal transformation of the geographical coordinates. At the present stage of model development and availability of computer capacities, the disadvantages of an inhomogeneous horizontal grid are easily outweighed by its advantages. For one, polar singularities are avoided by transformation of the model poles to a continental site. Secondly, the spatial inhomogeneity of the horizontal grid allows high resolution in regions of interest (up to 25 km for the Arctic Ocean in the present case) while low resolution is accepted for remote regions (300 km near the equator in the present case). This design avoids well-known open boundary problems of fine-resolution regional or nested models.

While the low-resolution regions provide a model-consistent climatology, the high-resolution regions admit even the study of mesoscale processes. In spite of this versatility, the machine requirements for GROB HOPE are those of a global model with a spatially homogeneous $3^{\circ} \times 3^{\circ}$ grid. This design permits a time step of 2.4 hours. With its coarse spatial resolution in the tropics, the GROB version of HOPE does not especially qualify for El Nino simulation. It is here to be shown that assimilation of observations is able to offset these design limitations. Success in this framework provides a demonstration of the capacities of sequential assimilation. For operational purposes, on the other hand, data will always be assimilated into the best model available.

In long term experiments (integration time: 1000 years) with climatological forcing resolving the annual cycle, the model assumes an essentially drift-free cyclostationary state after a few centuries which reproduces the major water masses and gyre structures of the global ocean circulation as well as the sea ice cover and its seasonal variation at high latitudes. While this model circulation exhibits the characteristic degree of realism of state-of-the-art simulations it also displays a number of typical deficits. The model fails to maintain the observed Pacific Intermediate Waters. Furthermore, while the pole ward Atlantic heat transport is certainly of the observed order of magnitude, its maximum of 0.8 PW is still somewhat lower than the 1.1 PW suggested by observations. On the other hand, the mass transport by the Antarctic Circumpolar Current with 180 Sverdrup in the Drake Passage is higher than the observed 140 Sverdrup. The path of the Gulf Stream, which is crucial for the European climate and weather, turns out to be quite sensitive to the details of the atmospheric forcing and the chosen parameterisation of subscale transports. For an extensive discussion of the strengths and weaknesses of the GROB HOPE circulation see Marsland et al. (2002).

4 The assimilation methods

4.1 Variational methods

Variational assimilation, namely the Adjoint Method, is based on an application of inverse modelling techniques to the estimation problem. Variation of control parameters minimizes a cost function formed by the model-data misfit. This approach lends itself particularly to the estimation of equilibrium states and processes of finite duration. Computation of the cost gradient with respect to the controls calls for what is often referred to as the temporally backward integration of the adjoint model (see Figure 8). For complex models, coding of the model adjoint is a substantial task, well comparable to coding the model itself. The practical relevance of adjoint assimilation in Earth System Modelling therefore arose only after the advent of the theory of automatic differentiation (Talagrand, 1991) and the subsequent development of automatic adjoint code compilers (Giering, 1996). Application of the Adjoint Method in state estimation with global circulation models is extensively discussed in (Ghil and Malanotte-Rizzoli, 1991; Malanotte-Rizzoli, 1996 and Ghil et al, 1997, see also Wunsch, 1997, and Giering, 2000, for a review).

DATA ASSIMILATION: THE ADJOINT METHOD

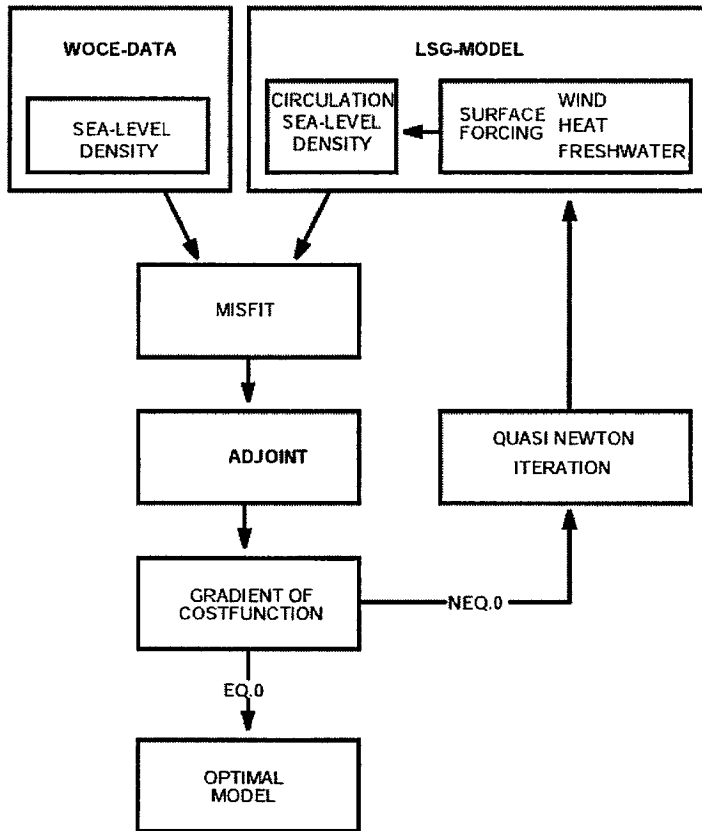


Figure 8: Schematic diagram of the Adjoint technique

4.1.1 Control Variables and Cost Function

The variational problem is to find a solution of the model equations and control variables X that minimizes the total cost function J_{TOT} over some temporal and spatial domain. J_{TOT} is defined by a summation of the data cost function J_D and the penalty cost functions J_p and J_w at time t and grid location ijk . The data cost function describes the distance between the space-based data Y^{sat} and the simulated model values Y . Penalty terms J_p are introduced to penalize differences between the first guess Y_F and current model values Y of sea surface temperature, differences from the SAC climatology Y^{cli} , differences from the first guess vertical velocities w_F .

If model equations are assumed to be perfect, i.e. no model error is included, then the optimised trajectory simulated by the model depends only on the initial conditions at time $t=t_0$, on the boundary conditions, and on the observations. J_{TOT} can thus be written:

$$J_{TOT} = J_D + J_P$$

$$J_D = \sum_t \sum_{ijl} R_{ij}^{sat} (Y_{t,ijl} - Y_{t,ijl}^{sat})^2$$

$$J_P = 1/2 \sum_t \sum_{ijk} R_{ijk}^{cli} (Y_{t,ijk} - Y_{F,t,ijk})^2 + 1/2 \sum_t \sum_{ijk} R_{ijk}^{cli} (Y_{t,ijk} - Y_{t,ijk}^{cli})^2 + \sum_t \sum_{ijk} P_{ijk} (w_{F,t,ijk} - w_{t,ijk})^2$$

with weights

$$\begin{aligned} R_{ij}^{sat} &= W_{ijl} \sigma_{sat}^{-2} \\ R_{ijk}^{cli} &= W_{ijk} \sigma_{cli}^{-2} \\ P_{ijk} &= W_{ijk} \sigma_w^{-2} \end{aligned}$$

We decided to modify effective air temperature T^* and effective surface salinity S^* to generate a synthesis of dynamically interpolated climatological and space-based observations. The air temperature T^*_{air} describes the heat exchange as a function of wind stress and surface air temperature (see Maier Reimer et al., 1993). The effective surface salinity S^*_{air} is essential related to the freshwater flux (precipitation minus evaporation). This assumption is derived from previous experiments with the inverse model (Mueller et al., 1998; Wenzel et al, 2001). The weighting matrix R^{sat} denotes the observation error covariance matrix, which we assume to be diagonal, i.e., that the data are independent and normally distributed. For the standard deviation of satellite data σ_{sat} we used a value of $\pm 0.125^\circ\text{C}$ consistent to the 8-bit resolution of the space-based observations.

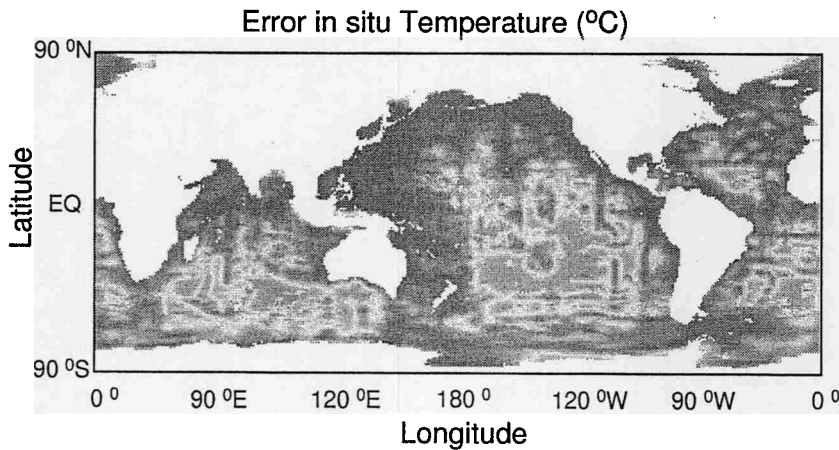


Figure 9: Standard deviation σ_{cli} of the annual mean climatology of sea surface temperature of marine in situ observations from WOCE special analysis center (SAC). Color ranges from 0.05°C (dark blue) to 1°C (red).

Values of covariance matrix for R^{cli} with standard deviation σ_{cli} have been taken from Gouretski and Jahncke (1998) (Figure 9). The matrix P contains the standard deviation of the vertical velocity σ_w and is calculated from the seasonal variance for modern times. The weight W_{ijk} is the ratio of the volume on the location ijk of the misfit between model value

and observation and the correlation volume over which individual ocean measurement can be considered as representative.

4.1.2 Minimization Algorithm

A descending algorithm, the M1QN3-Module from Gilbert and Lemarechal (1989), which is a limited-memory quasi-Newton-Method (QN), has been used to calculate the corrected control variables - the new guess. With this guess a new cost function and gradient can be calculated. The descending procedure is successively continued until a minimum is found. The M1QN3-Module computes a local approximate Hessian matrix from the gradients of the cost function. Thus, a much higher convergence rate in finding a minimum can be reached in comparison with the conventional conjugate gradient method.

One of the major problems in applying the optimization technique to an OGCM is the successful search for a global minimum of the cost function. Thus, it is desirable to produce a first guess to be close to the global minimum to reduce the likelihood for a convergence in a local minimum. There are systematic methods to reduce the possibility of a convergence in a local minimum like simulated annealing (Barth and Wunsch, 1990; Krueger, 1993) or the use of different initial conditions to confirm the finding of a global minimum (see e.g. Schiller and Willebrand (1995)). However, these methods are currently too expensive in numerical and computational costs to allow an application to our adjoint model and there is no general guarantee in a complex nonlinear system that the absolute minimum will be found. Including these methods can be a future task to improve the performance of the assimilation scheme.

4.1.3 The Adjoint LSG-Model

The adjoint model has been constructed by inversion of the computer code of the forward model, a common technique for GCMs demonstrated by Talagrand (1991). With this method the statements of the forward model are transformed using the chain rule into a tangent-linear statement (the linearized code) and inverted into an adjoint statement. The structure of this inversion is generally systematic and thus automatic procedures can be applied. The adjoint Hamburg LSG has partly been generated by the tangent-linear and adjoint model compiler (TAMC) (Giering and Kaminsky, 1996).

The direct inversion of the model code presented here has some major differences to an earlier version of the adjoint LSG compiled by Giering (1996) due to further development of the forward model (e.g. different treatment of the calculation of the baroclinic velocities, changes in the ice model, and incorporation of tracers and biogeochemistry) as well as different treatment for implicit loops in the adjoint model code.

The correctness of the gradients produced by the adjoint model can be tested by a finite-difference estimate by a perturbation of the boundary and initial conditions of the forward model (Long, pers. comm.; Winguth, 1997). In addition, identical twin experiments provide information about the solution of the inverse approach.

4.1.4 The Adjoint C-HOPE

The purpose of our study is to develop an-state-of-the-art inverse high resolution primitive equation ocean model for climate monitoring to compute climatic variability and trends on the interannual and decadal time scale with an optimal fit to the hydrographical and remote sensing data. For operational monitoring of the climate system and detection of climate change, it is necessary to optimize:

the parameterisations,

the initial conditions

the forcing boundary conditions of the ocean general circulation model suitable for climate prediction.

The adjoint C-HOPE is suitable to accomplish all three improvements simultaneously, assuming that the computational resources are available. In this chapter we will describe the development of the adjoint C-HOPE.

4.1.4.1 Practical Coding of the Adjoint Model

It is useful for the understanding of practical coding of an adjoint model to explain the technique on a general example (Talagrand, 1991; Winguth, 1997).

The model equations (1)-(8) described as finite-dimensional algebraic cases in section 3.1. can be written as a dynamical system

$$\frac{dx}{dt} = F(x) \quad (10)$$

where we assume that x belongs to the \mathbb{R}^4 , the 3 spatial dimensions and one temporal dimension. The input is the initial condition $x(t_0)$, while $x(t_1)$ is the output of the integration of (10) at a given time $t_1 > t_0$. For a given solution $x(t)$ of (10), the corresponding tangent linear equation for a perturbation $\delta x(t_0)$ is given by

$$\frac{d\delta x}{dt} = F'(t)\delta x \quad (11)$$

where $F'(t)$ denotes for any t the Jacobian of the function F , taken at point $x(t)$.

The adjoint equations can be described as an integration from the final condition $\delta' x(t_1) = \nabla J$, the gradient of the cost function, of the adjoint equation

$$\frac{d\delta' x}{dt} = -F'^T(t)\delta' x \quad (12)$$

The description below requires the availability of both the numerical model of the ocean circulation model and of the adjoint model. The complexity of the adjoint C-HOPE (Figure 5) is comparable with the one of the direct (forward) model (Figure 3). The latter is under permanent evolution and constantly a subject of modification. Two principles have to be considered to develop the adjoint code, the principle of locality and readability: First, whenever a local modification is made on the direct code, the corresponding modification must be made in the adjoint code, and second, the first requires readability, meaning that when a local modification is made on a direct code, it must be easy to locate the place where the corresponding modification is to be made in the adjoint code.

These two principles require that the adjoint code must be generated directly from the direct code (and not, for example, from the partial differential equations on which the direct code is built). We shall illustrate these principles on an example FORTRAN statement from the subroutine BUDGET in C-HOPE, e.g. the computation of the incoming heat flux by solar radiation:

$$\begin{aligned} &\dots \\ &Q2(N) = (1.-ALB1(N)) * SLN1(N) \qquad (13) \\ &\dots \end{aligned}$$

The input to this statement is made up of ALB1(N) and SLN1(N), while its output is made up not only of Q2(N) but also of ALB1(N) and SLN1(N).

The corresponding "tangent linear statement," analogous to (13) reads

$$\begin{aligned} &\dots \\ &\square Q2(N) = (1.-ALB1(N)) * \square SLN1(N) - \square ALB1(N) * SLN1(N) \qquad (14) \\ &\dots \end{aligned}$$

which, for given ALB1(N) and SLN1(N) (i.e., for a given basic solution), defines a linear operator with input $(\square ALB1(N), \square SLN1(N))^T$, and $(\square Q2(N), \square ALB1(N), \square SLN1(N))^T$. The corresponding matrix is the 3 x 2 matrix

$$\begin{array}{cc} -\text{SLN1(N)} & (1.- \text{ALB1(N)}) \\ 1 & 0 \\ 0 & 1 \end{array}$$

The corresponding adjoint computation, from a 3-vector $(\square Q2(N), \square ALB1(N), \square SLN1(N))^T$ to a 2-vector $(\square ALB1(N), \square SLN1(N))^T$ will therefore read

$$\begin{aligned} &\dots \\ &\square ALB1(N) = \square ALB1(N) - \square Q2(N) * SLN1(N) \\ &\square SLN1(N) = \square SLN1(N) + \square Q2(N) * (1. - ALB1(N)) \qquad (15) \\ &\dots \end{aligned}$$

$\delta Q2(N)$, $\delta ALB1(N)$, and $\delta SLN1(N)$ are the partial derivatives of the output function of the direct code with respect to the variables contained in the respective addresses Q2(N), ALB1(N), and SLN1(N) after statement (13) has been executed, while $\delta ALB1(N)$ and $\delta SLN1(N)$ are the partial derivatives of the same output function with respect to the variables contained in addresses ALB1(N) and SLN1(N) before statement (13) has been executed. Experience shows that it is more convenient to use the same variable name for a variable of the direct code. According to simple transparent rule by adding an AD in front of the variables, equation (15) will be transformed into

$$\begin{aligned} &\dots \\ &ADALB1(N) = ADALB1(N) - ADQ2(N) * SLN1(N) \\ &ADSLN1(N) = ADSLN1(N) + ADQ2(N) * (1. - ALB1(N)) \\ &ADQ2(N) = 0. \qquad (16) \\ &\dots \end{aligned}$$

The structure of this inversion is generally systematic and thus automatic procedures can be applied. A more detailed discussion on how to generate an adjoint computer code and its au-

automation by the Tangent-linear and Adjoint Model Compiler (TAMC) is given in Giering and Kaminski (1996). The statements of the forward model are transformed using the chain rule into a tangent-linear statement (the linearized code) and inverted into an adjoint statement. Here, we modified C-HOPE to be readable for the TAMC (e.g. remove non ANSI FORTRAN statements). In a second step, we compiled the subroutines of the time loop of C-HOPE with the TAMC. In a third step we optimised the code produced by TAMC to be computationally efficient. The flow chart of the adjoint model's time loop is shown in Figure 5. An example program is given in Appendix A.

The correctness of the gradients produced by the adjoint model can be tested by a finite-difference estimate by a perturbation of the boundary and initial conditions of the forward model (Appendix B). In addition, identical twin experiments provide information about the solution of the inverse approach and will be the subject of future tasks.

4.2 The Kalman-Filter-Method

Sequential methods such as the Kalman Filter are specifically tailored to the needs of monitoring and prediction (Jazwinski, 1970). These updating schemes emerge from the application of the theory of stochastic processes to estimation and yield an estimate of minimum variance. On update, the relative weight of model and data is determined by the Kalman Gain which is computed from data and model error dynamics (see Figure 11). To this end, the model error is considered as a stochastic process. The dynamics of such processes can be equivalently formulated in the Langevin (or Heisenberg) representation and in the Fokker-Planck (or Schrödinger) representation (van Kampen, 1981) The Langevin picture addresses the space-time behaviour of the process in terms of its moments. In practice, this refers generally to the covariance only. Formally, the temporal development of the covariance is uniquely determined by the model dynamics. However, the practical derivation of the covariance dynamics for a complex model such as a global ocean circulation model readily becomes everything but straightforward.

This applies particularly to non-linear models, the issue of boundary and initial conditions for the covariance, stability questions and the problem of temporally backward assimilation. Nevertheless, at this time the literature on Kalman Filter assimilation in Earth System Modelling and other branches of engineering is almost exclusively dominated by the Langevin approach (Ghil et al, 1997).

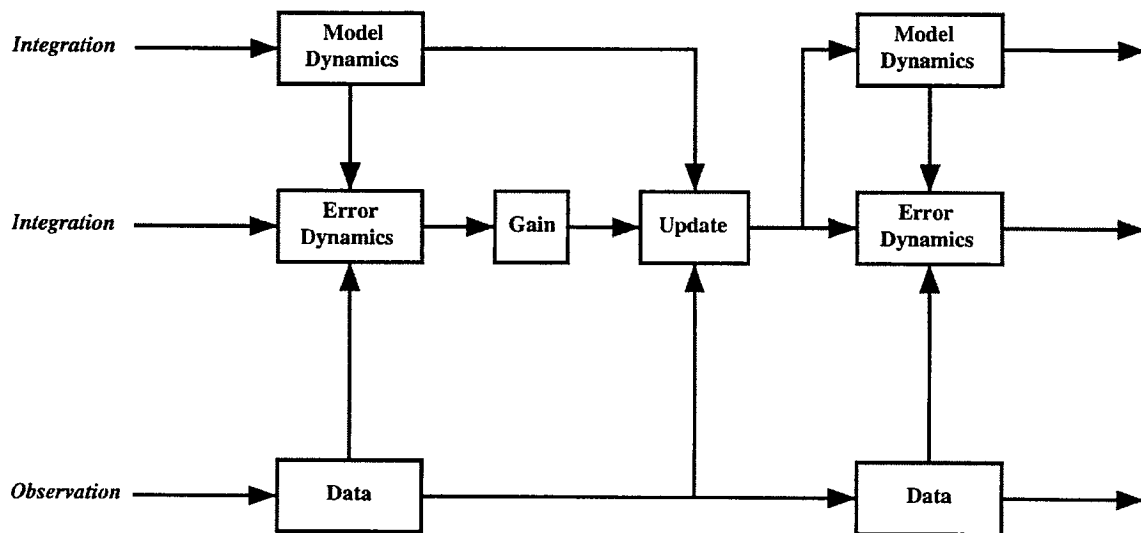


Figure 11: Flow Chart of Sequential Assimilation

Alternatively, a stochastic process may be considered in phase-space in terms of its probability density. Provided the process is Markovian and jumps remain small in an appropriate sense (van Kampen, 1981) the dynamics of this probability density are governed by the Fokker-Planck Equation. The advection- and diffusion-coefficients of this linear parabolic differential equation are determined by model dynamics and observational error statistics. In general, these coefficients are also difficult to obtain from a complex model. However, for sufficiently short update intervals, phase-space advection and diffusion can be determined phenomenologically from the model output by histogram techniques.

In this framework, the assimilation method provides practical answers to the issues of phase-space reduction, model nonlinearity, initial and boundary conditions for higher moment dynamics as well as stability. Moreover, the existence of the Backward Fokker-Planck Equation (van Kampen, 1981) will permit the generalization of sequential assimilation to include the temporally backward extrapolation of data information. The mathematical aspects of the Fokker-Planck representation of sequential Kalman Filter assimilation have been developed in detail by Belyaev et al (2001).

With the typical volume of model output and observational record in Earth System Modelling, computational demands for assimilation with least-square optimality are always quite high. For a reduction of the computational burden, the present estimation utilizes a combination of Kalman Filter assimilation and simple “nudging”. While subsurface temperatures from the TAO/TRITON array will be assimilated sequentially, observations of global sea-surface temperatures are essentially inserted into the model at daily intervals. The feasibility of this simplistic technique is by no means trivial. Older model generations were generally unable to “digest” essentially unprocessed data and model-data inconsistencies would readily emerge in various regions of space-time and phase space. It will here be shown that the quality of contemporary models and data sets is sufficiently high for nudging to be beneficial for the ocean state estimate.

5 Results

5.1 Experiments with the LSG-Adjoint model

Based on observed radiocarbon differences between the surface and the deep-sea, OGCMs are generally spun up a couple of thousand years to simulate the steady state of the ocean circulation. However, past computational capacities limited the integration of inverse OGCMs to a length in the integration times of less than a few decades. Marotzke and Wunsch (1993) discussed the quality of the assimilation as a function of integration time of the inverse OGCM and concluded that an increase in the integration interval would considerably improve the reconstruction of non-linear processes such as convective mixing, sea ice formation, and biogeochemistry and would hence improve the quality of the deep-sea circulation and tracer distribution. Results from identical twin experiments (Winguth, 1997) suggest that the decline of the cost function is strongly dependent on the length of the integration time for the inverse ocean model because longer time scales in the ocean circulation are more adequately represented with increasing integration time.

5.1.1 Climatological Reference Run

In order to create a reference for the data assimilation, a reference and first guess experiment has been carried out by restoring the surface layer to monthly mean ECMWF reanalysis air temperatures and wind stress annual mean surface salinities (Levitus, 1982). Here, we have taken the flow field of the interglacial first guess (IFG) experiment of Winguth et al. (1999) as an initial condition. The model has been integrated for about 4000 years into a cyclostationary steady state. The Atlantic overturning circulation at 30 °S is about 3-5 Sv weaker than in experiment ATOS1 (Atmospheric Temperature, Ocean Salt and atmospheric temperature advection with reference factor 1) produced by Maier-Reimer et al. (1993) or the IFG run carried out by Winguth et al. (2000). These findings are consistent to recent tracer-based estimates of Broecker et al. (1998) and also to previous assimilation experiments of Winguth et al. (1998) in which active tracers (temperature and salinity), radiocarbon and PO₄* have been assimilated into a large-scale geostrophic model. Here, an increase in surface temperature relative to IFG in the North Atlantic causes a decrease in convective overturning, a decrease in the North Atlantic deep circulation (Figure 12), and an increase of the inflow of Antarctic Bottom Water.

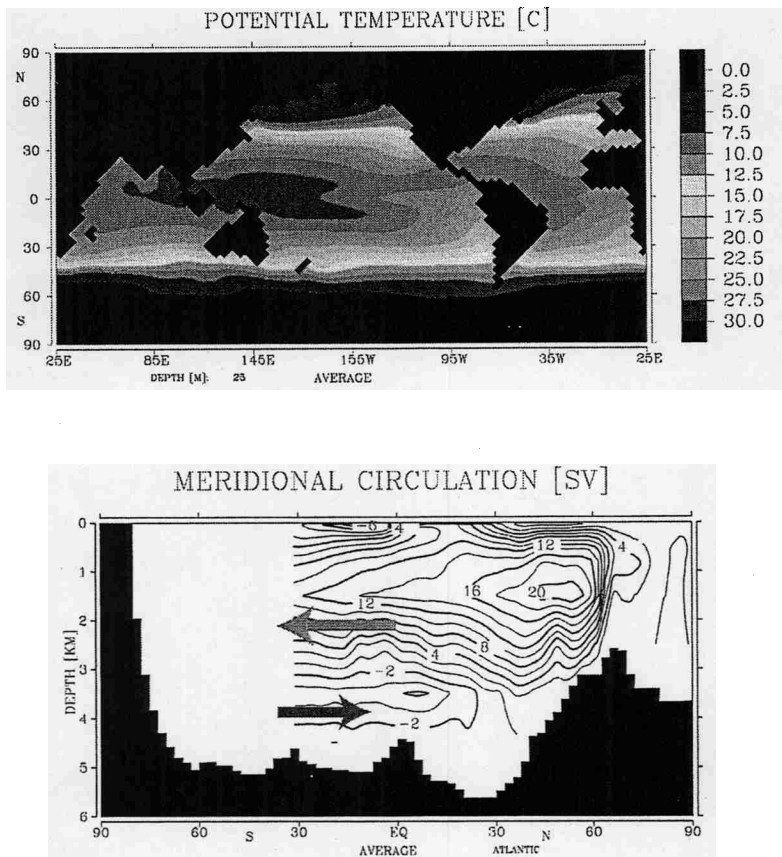


Figure 12: Climatological reference run with a large-scale ocean circulation model as a response to ECMWF-reanalysis boundary conditions. (a) Sea surface temperatures and (b) meridional overturning circulation of the Atlantic Ocean.

5.1.2 Identical Twin Experiment

Two assimilation experiments are required for this study: An identical twin experiment to validate the inverse model and an assimilation experiment with the data sets described above. An identical twin experiment is carried out by running the inverse model with “data” generated from model experiments by perturbations in the forcing surface boundary conditions. It represents the best possible solution for the adjoint approach because the “data” generated by a perturbation experiment with the forward model are compatible with the optimised model results. A detailed description of the validation of the inverse model is described for example in Thacker and Long (1988), and for the inverse LSG in Giering (1996) and Winguth (1997). Effective air temperature T^*_{air} is perturbed by an anomaly, which consists of a spatial pattern orthogonal to the model topography with randomly generated amplitudes (Figure 7a; see also Winguth, 1997) and is used together with salinity and wind stress from the reference run as a perturbed forcing boundary condition.

The model has been integrated with these forcing fields for 10 years to generate a perturbed distribution of temperature and salinity. The reproduction of the forcing anomalies by assimilation of the hydrography generated by the perturbation experiment into the adjoint model is documented by a significant reduction of the cost function (Figure 13).

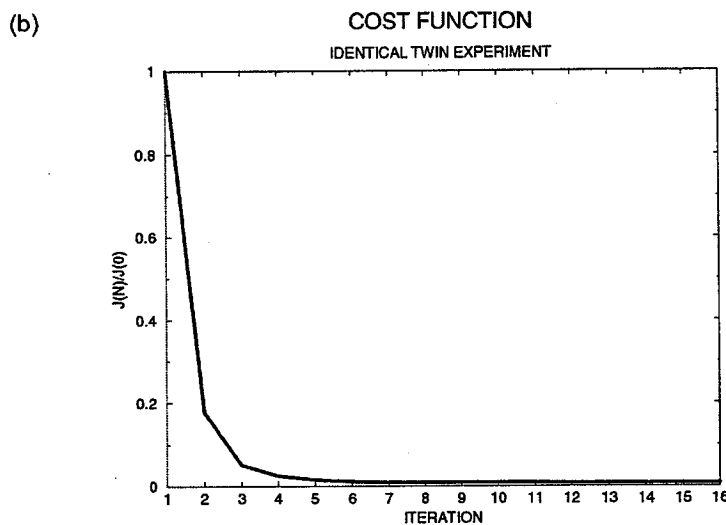
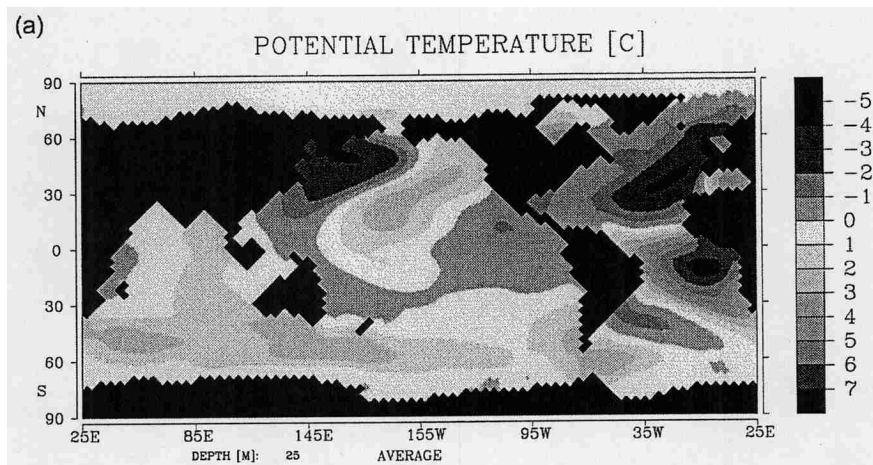


Figure 13: Identical twin experiment with an adjoint large-scale ocean circulation model. (a) Randomly generated anomaly of effective air surface temperature (T_{air}^*) for year 10 and (b) normalized cost function by assimilation of the SST of (a) into the adjoint model.

5.1.3 Satellite Data Assimilation Experiment

We used the adjoint LSG with the data sets described above: MCSST satellite data were taken for the El Niño year 1998 to test the response to extreme natural variability with an extreme event. Constraints on the solution were given by the use of SAC climatology (section 2.3.) and the first guess flow field in response to ECMWF-Reanalysis surface climatological wind stress and surface temperatures from Section 2.2. The optimised circulation is displayed in Figure 8a. The optimisation procedure has been applied 13 times until changes in the different contributions of the cost function were smaller than 1%

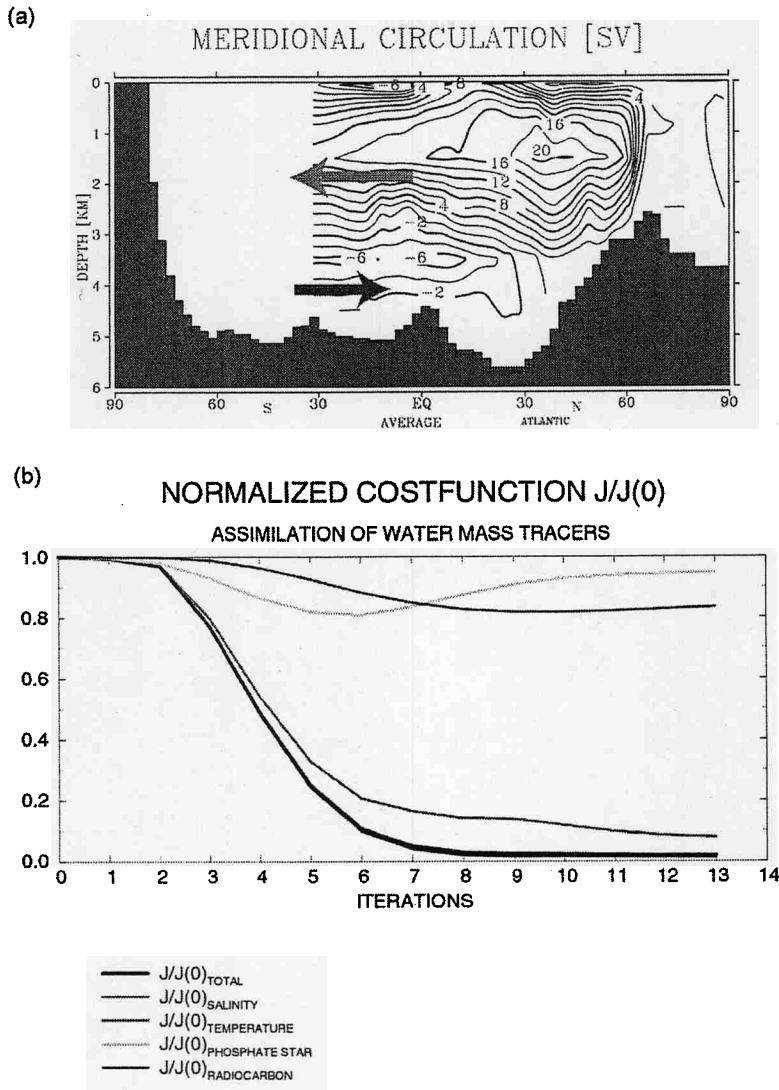


Figure 14: (a) Optimised overturning circulation of the Atlantic Ocean from assimilation of space-based and in situ observations into an adjoint large-scale ocean circulation model. (b) Normalized total cost function and changes of the model-data differences of the tracers (salinity, temperature, PO_4^* and radiocarbon).

(Figure 14). The optimised modern circulation and buoyancy fluxes reproduce the general features of pronounced anomalies during the El Nino Year 1998 with a strong sea surface temperature anomaly of about 4°C in the Eastern Equatorial Pacific. Simulated amplitudes are somewhat lower than the satellite data related to climatological first guess forcing fields. The results suggest an export flux of about 15 Sv from the North Atlantic Deep Water into the Southern Ocean. Our results are in agreement with the interpretation of the distributions of the carbon-14/carbon-12 ratio and a quasi-conservative property, PO_4^* , in the deep sea (Broecker et al., 1998). A major reduction in Southern Ocean deep-water production during the 20th century (from high rates during the Little Ice Age) may explain an apparent discordance of PO_4^* and radiocarbon measurements to recent CFC-12 measurements (Broecker et al., 1999).

The positive buoyancy anomaly in the North Atlantic causes an increase in convective overturning, and an increase in the North Atlantic deep circulation (Figure 8a). However, recent coupled experiments with a climate model (Banks et al., 2000) indicate a large internal variability in northern hemisphere oceans, and a signal of anthropogenic climate change is not detectable within in the next 20 years of future projections. These simulations suggest that southern hemisphere changes in turn are potentially a sensitive indicator of anthropogenic climate change and, together with the North Atlantic, might be an important part of climate monitoring network.

5.1.4 Cyclostationary Global Circulation Estimation

The adjoint approach is also used to estimate the cyclostationary global ocean circulation by synthesizing the dynamics of the Hamburg LSG Model with temperature and salinity.

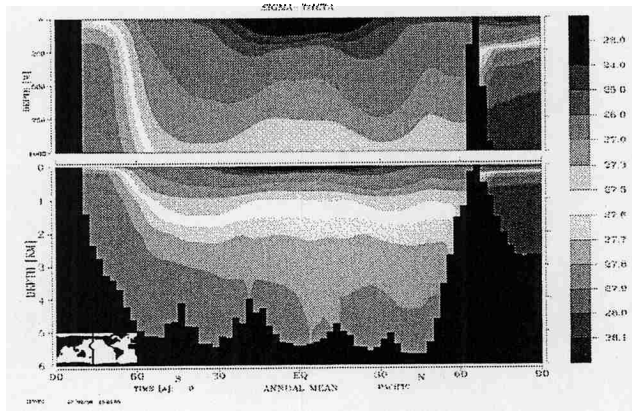
The database for the present state estimation are the unprocessed station data of the World Ocean Atlas (Levitus et al, 1998)} for the period from 1970 to 1993. These data are discretized on a $2^0 \times 2^0$ grid with 29 levels in the vertical and monthly means are taken at each data grid point. Monthly mean temperature- and salinity-profiles are checked for static stability and discarded if unstable. Additional smoothing or filtering is not applied. These data provide a statically stable, mean annual cycle of the global oceanic buoyancy field at a time step of one month. Data variances are calculated from the raw data and the atlas-average is substituted where only one datum is available. Model-data misfit and cost function are calculated by projection of the model hydrography onto the data grid to minimize the corruption of data information in the essential link of model and data.

Figure 15 shows the result of the state estimation for an annual mean cross section of the density variable sigma-theta through the Pacific. Figure 15a depicts the data of the World Ocean Atlas. The data show a well-stratified body of fluid with the characteristic upwelling signature near the equator. The simulation of this density field by the LSG Model without assimilation is shown in Figure 15b. Obviously, the model captures the basic stratification together with the upwelling signature near the equator quite realistically. However, it fails to produce the very heavy bottom water that is produced in high Southern latitudes. In combination with the data, the LSG Model is seen in Figure 15c to be able to produce this water mass in realistic quantity and distribution

Figure 16 shows the annual mean surface heat flux before (Figure 16a) and after (Figure 16b) the assimilation. Warm colours indicate the heating of the ocean by the atmosphere and cold colours a heat loss of the ocean to the atmosphere. Particularly in the North Atlantic, the heat flux distribution is significantly more realistic after the assimilation.

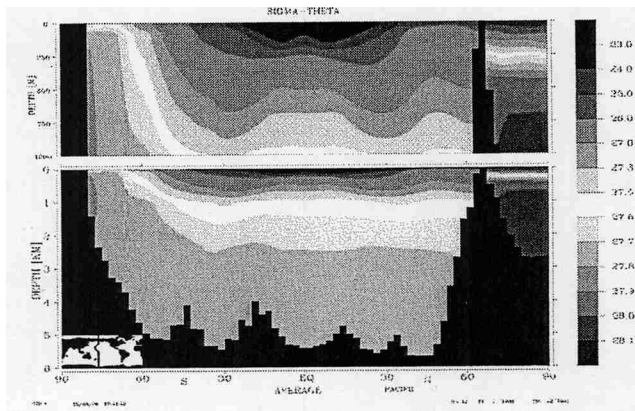
WOA RAW DATA

Fig. 15a)



LSG BEFORE ASSIMILATION

Fig. 15b)



LSG AFTER ASSIMILATION

Fig. 15c)

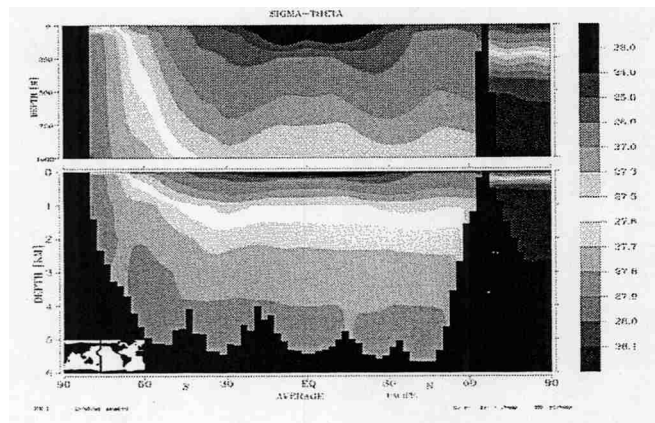


Figure 15: The state estimation for an annual mean cross section of the density variable sigma-theta through the Pacific. a) data of the World Ocean Atlas. b) the simulation of this density field by the LSG Model without assimilation; and c) after assimilation.

Abb. 16a)

LSG BEFORE ASSIMILATION

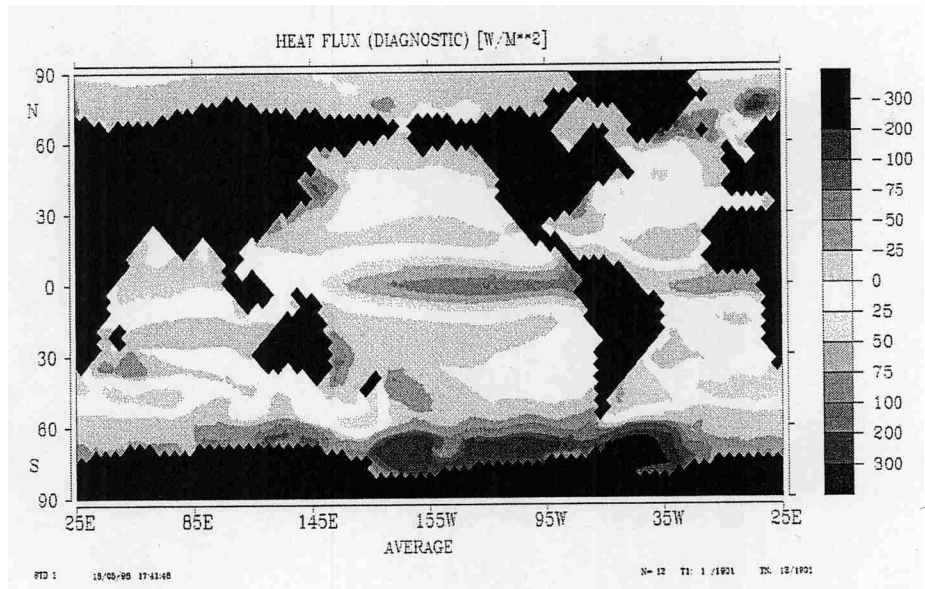


Abb. 16b)

LSG AFTER ASSIMILATION

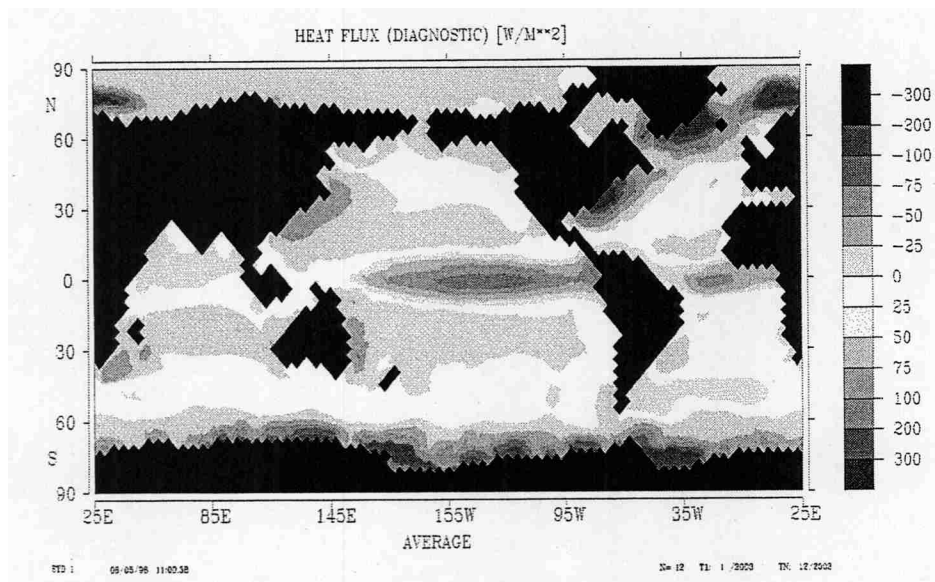


Figure.16: The annual mean surface heat flux before (a) and after (b) the assimilation. Warm colours indicate the heating of the ocean by the atmosphere and cold colours a heat loss of the ocean to the atmosphere.

5.2 Kalman-Filter assimilation with the GROB-HOPE model

The key idea of sequential assimilation is to integrate the model until an observation becomes available. At this time, model integration is halted and the state of the system is updated by an appropriate combination of model prediction and observation. Subsequently, this update provides the initial value for the continued model integration. Hence, the main task in sequential data assimilation is the determination of the temporal development of the relative weight of model prediction and observation. In the phase space representation of the Kalman Filter, this problem is solved by integrating (a large number of) simple, 2+1 dimensional Fokker-Planck equations which account for model dynamics in terms of phase space advection and diffusion. Determination of these parameters by an elementary histogram technique circumvents a number of quite complex, but essentially technical issues of the stochastics of non-linear systems. In numerical applications, the method proves efficient and reliable (Belyaev et al, 2000, 2001).

The feasibility of operational global ocean state estimation will here be demonstrated by combining simulations of the numerical circulation model GROB-HOPE with observations of global sea-surface temperatures (SST) and observed subsurface temperatures from the TAO/TRITON array for the El Nino year 1997. Besides a globally realistic mean state, the objective of the estimate is the improvement of the model's El Nino simulation.

After an initial spin-up period of 2 years with restoring to the 3-dimensional buoyancy climatology of WOA the model is integrated from 1948 to the present with surface forcing derived from the NCEP reanalysis (Kalnay et al, 1996). Atmospheric data are interpolated onto the GROB HOPE grid and surface buoyancy- and momentum-fluxes are calculated by bulk formulae (Marsland et al., 2002) depending on both, the atmosphere and the ocean. Hence, the eventual ocean forcing is determined by the particular realization of the ocean state by the model while the present ocean-only set-up is unable to account for a feedback of the ocean on the atmosphere. For a reduction of trends in the deep ocean, integration over the NCEP period is repeated. Furthermore, model surface salinities are nudged to a mean annual cycle taken from WOA with a time constant of a little over a year (385d). Use of a mean annual cycle rather than an annual mean accounts for the seasonal variation in the hemispheric distribution of convective activity. With this forcing the model is integrated to 31 December 1997. The period from 1 January 1997 to 31 December 1997 is taken as the control run in the present experiment and the model state at 31 December 1996 provides the initial condition for the assimilation. It is noted that model runs considered here do not address the prediction problem. Surface data transfer external El Nino information to the ocean model.

Figure 17 shows the monthly mean of the net surface heat flux of the control configuration for December 1997. This heat flux is determined by atmospheric data from the NCEP reanalysis and oceanic data from GROB HOPE. The main feature is the characteristic seasonal separation of the (southern) summer- and (northern) winter-hemisphere: the ocean gains heat in summer and loses heat during winter. A particular detail in the North Atlantic is associated with model problems in simulating a realistic Gulf Stream path: off the American east coast,

the ocean is unrealistically warm leading to a pronounced heat loss while the ocean is unrealistically cold in the region of the so-called North West Corner leading in turn to a pronounced heat gain by the ocean. Similar aberrations are seen in the Kuroshio region, the confluence of the Malvinas and Brazil Currents off the South American east coast and for the Agulhas Current near the Cape of Good Hope. The paths of these currents are essentially determined by vorticity dynamics and mismatches of NCEP derived forcing and model simulation is due to ambiguities in the vorticity dynamics of the Primitive Equations. Given the NECP fluxes, GROB HOPE fails to simulate meso-scale details of the state of the underlying ocean surface realistically.

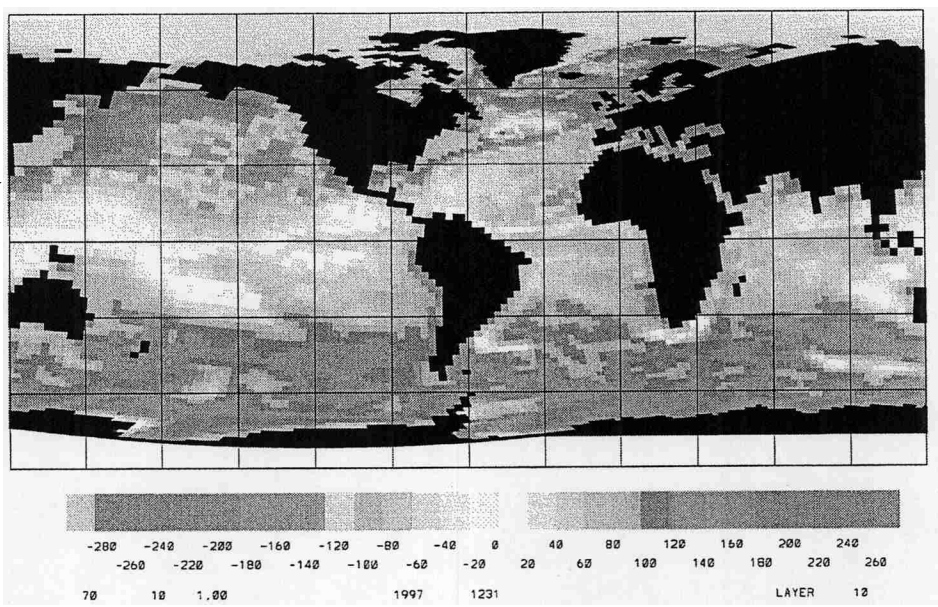


Figure 17: The Monthly Mean Surface Heat flux for December 1997 [Wm^{-2}] of the CONTROL experiment.

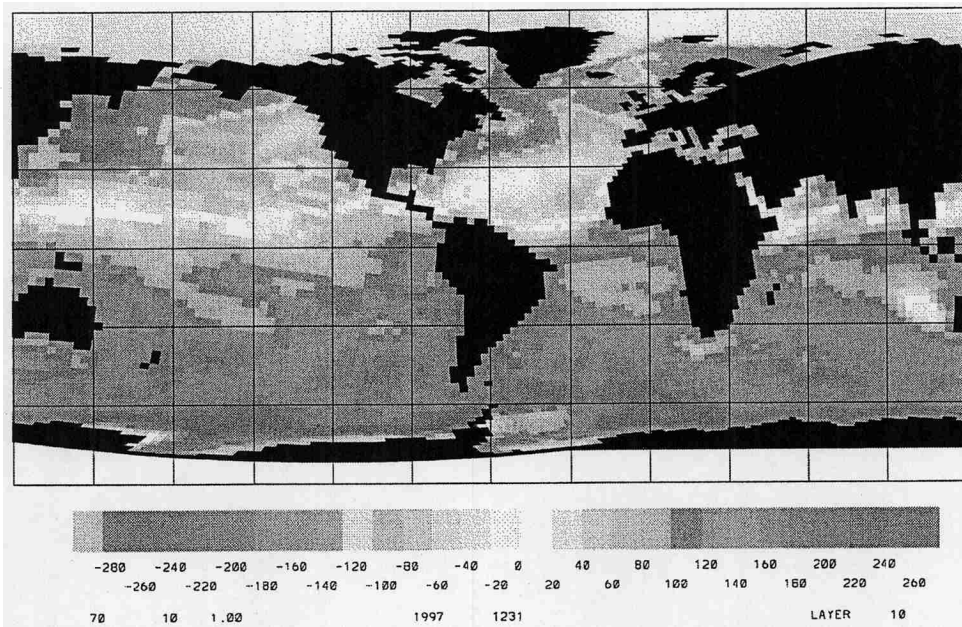


Figure 18: *The Monthly Mean Surface Heat flux for December 1997 [Wm^{-2}] of the NUDGE experiment*

It is shown that nudging of observed SST into the model improves the state estimate considerably. To this end, GROB HOPE is restarted from 31 December 1996 and daily mean Reynolds SST of the NCEP data set are inserted into the model's top layer at a time constant of one day. During this one-year integration, model-data incompatibilities do not develop. This is also true for GROB HOPE runs with SST nudging over the full NCEP period (not shown). Figure 18 depicts the monthly mean net surface heat flux for December 1997 with SST nudging. In comparison to Figure 17, it is seen that aberrations of the major current systems are significantly reduced and the estimate of meso-scale features of the state of the sea surface improves without penalty.

Nudging effects are not confined to the upper ocean alone. In convectively active regions surface temperature information is rapidly communicated to the abyss. For the present integration period of one year the deep ocean remains of course unable to adjust to the "injected" information. Nevertheless, with these data and for this model, nudging becomes a practical option of ocean state estimation by an efficient and yet robust model-data combination. Other presently available observations are of similar quality: sea-level data from space-borne altimeters and space-based observations of sea-ice cover. By nudging observations of this type into a global ocean circulation model, it is currently possible to arrive efficiently at a comprehensive and realistic estimate of the global state of the sea surface at meso-scale resolution.

For the assessment of the state of the interior ocean consider the equatorial temperature field during the El Nino episode of 1997/98. Figure 20 shows the temperature difference NUDGE-WOA along the equator for December 1997 where "NUDGE" refers here to the GROB HO-

HOPE simulation of the global ocean circulation with NCEP forcing and nudging of daily SST observations, i.e. the run also portrayed in Figure 19.

In the abyssal Pacific, simulation and observation are seen to differ by typically less than half a degree. While the simulation is systematically colder than WOA, structural mismatches do not emerge. The agreement is less satisfactory in the abyssal Indic and Atlantic. In the near-surface Pacific, the model clearly exhibits the characteristic El Nino pattern. Relative to the WOA climatology, the eastern and central Pacific are colder while the West is anomalously warm. Comparison with observed subsurface temperatures (www.pmel.noaa.gov/tao/jsdisplay) shows that the model simulates the phase of the process quite realistically. Since phase information is directly provided by forcing data, this model response is primarily indicative of the consistency of the simulation of near-surface wave propagation with surface boundary conditions.

Other features of Figure 19 exhibit a lesser degree of realism. The warm anomaly in the surface waters of the central Pacific cannot be found in the observational record (www.pmel.noaa.gov/tao/jsdisplay)

Here, the mixed-layer model of GROB HOPE fails to mix the heat supplied at the surface, sufficiently deep into the upper ocean. In the model, heat mainly penetrates to greater depth by slow diffusion processes. In the ocean, however, these transfers are dominated by turbulent mixing. As another consequence of the mixing parameterisation, GROB HOPE underestimates mixed-layer depths throughout the year and thus fails to account for Kelvin wave downwelling during El Nino. Thermocline temperatures beneath the mixed layer are about 2^o Celsius too warm. Here, the model diffuses too much heat to depths of approximately 500m in the eastern equatorial Pacific, which penetrates westward at approximately 250m. This mismatch is the result of unrealistically strong downward diffusion of heat and unrealistically weak upwelling of cold waters.

For Primitive Equation models, non-hydrostatic mixing processes have to be parameterised and such parameterisations are by no means trivial. The mixed-layer model of GROB HOPE is tuned to yield realistic mixing depths at moderate latitudes and compromises for the equatorial mixed layer are accepted. The alternative would be a far more complex and machine-intensive mixed-layer model. Moreover, vertical velocities are determined from mass conservation, independent of the momentum budget. Possible problems and ambiguities are smeared out by diffusion. Hence, models have a tendency to use diffusion where space-time- and phase-space-characteristics of the real ocean are determined by advection and propagation.

Sequential assimilation of subsurface temperatures improves this state estimate significantly. Subsurface temperature data are taken from the TAO/TRITON array, which consists of approximately 70 moorings in the tropical Pacific between 8^o S and 8^o N. The buoys record a number of atmospheric parameters, sea surface temperatures and subsurface temperatures at 10 irregularly spaced depths in the upper 500m. Records are transmitted to shore in real-time via the ARGOS satellite system. TAO/TRITON has become one of the most successful ground-based ocean observatories.

Figure 20 shows the monthly mean temperature difference Assimilation-Nudge along the equator for December 1997. The data are seen to have three major effects on the estimate: the surface becomes colder, the mixed layer warmer and the thermocline colder. These modifica-

tions lead to a significantly higher degree of realism for the estimate. Assimilation ensures that heat supplied at the surface, is uniformly mixed into the upper layer and cold water is upwelled into the thermocline. In response to the data information, the model replaces diffusion-dominated dynamics with mixing and advection.

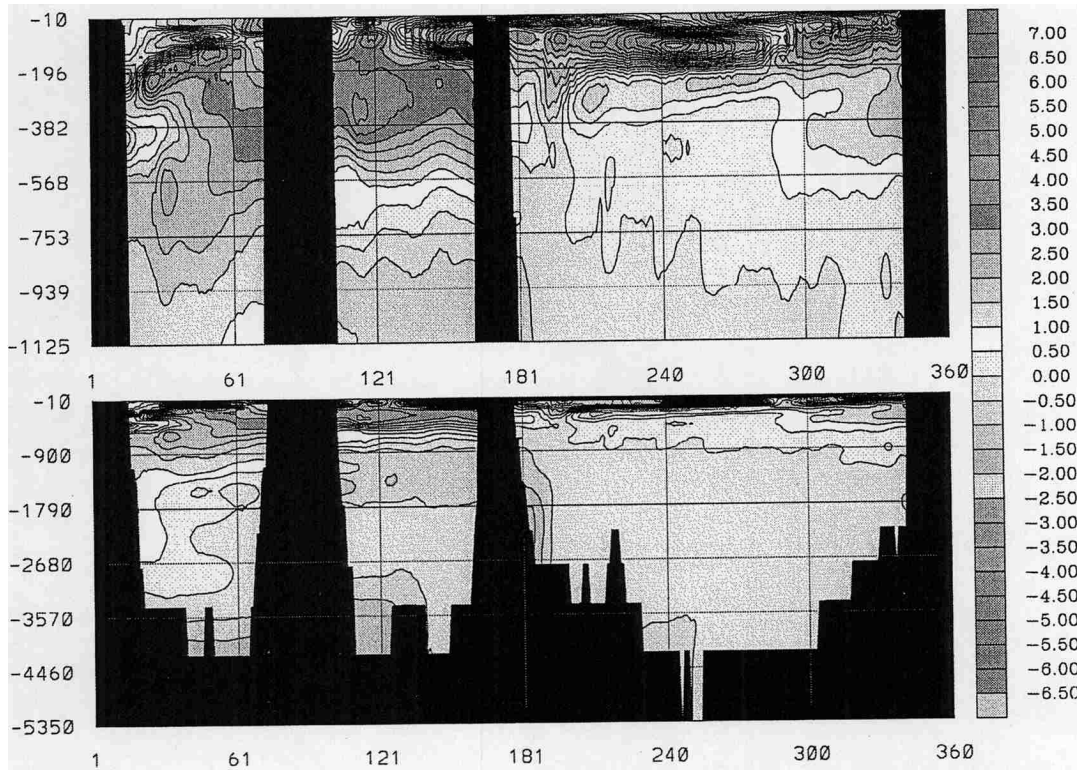


Figure 19 The Monthly Mean Temperature Differences on the Equator. December 1997. NUDGE - WOA

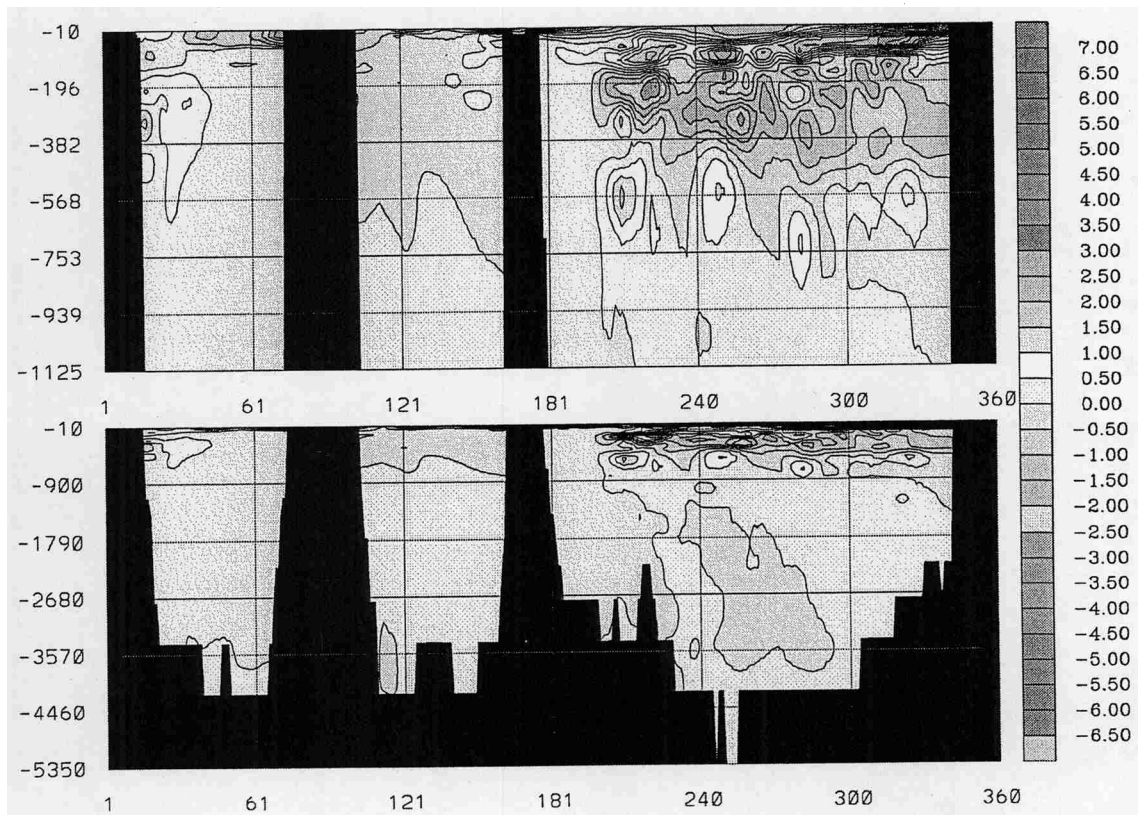


Figure 20: The Monthly Mean Temperatures differences on the Equator for December 1997. Assimilation – NUDGE

However, it is also seen that the assimilation still exhibits some pockets of warm water below 500m although far less than Figure 4. Primarily, these pockets are a consequence of the lower boundary condition chosen for vertical transition probabilities: the model is assumed to be true at 500m. Obviously, there is room for improvement.

A different view of these data effects is given in Figure 21. The figure shows a time series of monthly mean temperature profiles at a location in the eastern equatorial Pacific for 1997. Simulated (black) and assimilated (red) profiles are compared. The simulation is clearly diffusion dominated, unable to produce a mixed layer and leaking too much heat into the thermocline. The assimilation also fails to produce well-defined mixed layers during the first part of 1997. Before the arrival of the downwelling Kelvin wave in the eastern Pacific, mixed layers here are shallow (typically 25m). Their absence in the assimilation during the first part of the year is a consequence of the poor vertical resolution of GROB HOPE. With the arrival of the Kelvin wave, assimilation produces the characteristic signature of turbulent mixing in the upper ocean with realistic mixed-layer depth. At the same time, the thermocline is cooled by upwelling of colder water and temperature gradients at the mixed-layer base increase.

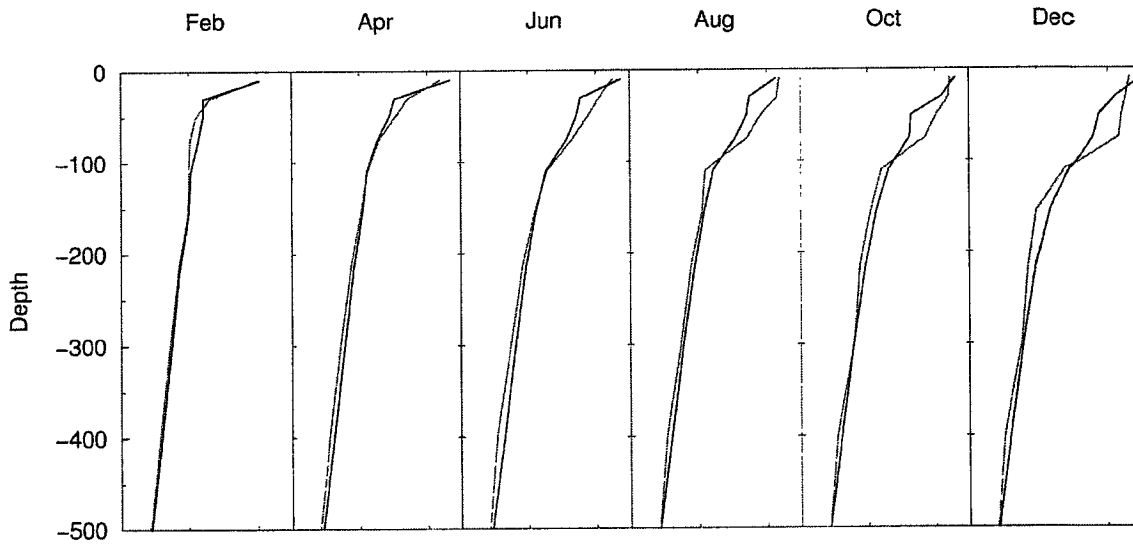


Figure 21: Time-Series ($\Delta t=2$ months) of Temperature Profiles in the Eastern Pacific during 1997. NUDGE (black), Assimilation (Red).

6 Summary

Ocean state estimation draws its wider societal as well as scientific significance from the central role of the oceans in Earth's climate system. At a time when the impact of climate variability on societal infrastructures is increasingly felt, the need for comprehensive climate monitoring is generally accepted. While mankind is primarily affected by meteorological manifestations of climate variability, large-amplitude weather fluctuations often screen the atmospheric climate signal. In practice, atmospheric climate observation proves prohibitively intricate. Alternatively, estimates of the state of the ocean interior with its enormous capacity to store and distribute water, heat and radiatively active trace substances (such as carbon dioxide) provide direct evidence of the climate signal. As the dominating climate component, the ocean acts as a Markov Integrator of atmospheric noise, provides the memory of the climate system and sets time-scales of climate processes by (at least partly) predictable transport mechanisms. Thus, practical climate monitoring anchors on operational ocean state estimation.

Novel ocean observation techniques provide a global data base for such estimates. For a number of parameters, these observations are available almost in real-time and at mesoscale resolution. Assimilators utilize numerical circulation models to dynamically extrapolate ocean observations in space-time and phase space and, at the same time, constrain model uncertainties.

In a pre-operational study, PRAOMS assimilated successfully a combination of data sets from different sources (space-based observations, hydrographical data, re-analysis values) with the adjoint version of the LSG-model and a sequential Kalman Filter of the GROB HOPE model.

Moreover, an adjoint version of the HOPE-C model had also been developed, but could not yet be tested. Assimilation experiments produced an optimal synthesis of different data sets consistent with the model representation of the laws of dynamics. Model-data differences between the initial model state and the observations have been substantially reduced. In an operational framework, the tested assimilators improve future climate and weather forecast quality.

Remaining residuals between model and data are related to the following uncertainties, which also determine the challenges for future work in the field:

- Model equations are assumed to be perfect and an explicit model error is not considered in the inverse formulation. The results strongly depend on the way the model is parameterised (e.g., internal friction, parameterisation of deep water formation, choice of numerical scheme, model resolution, formulation of the boundary conditions (Mikolajewicz and Maier-Reimer, 1994; Rahmstorf and England, 1997), or topography (McDermott, 1996)).
- Uncertainties within the space-based and in situ observations, the sparse spatial distribution especially in the Southern Ocean, and the assumption of the observational distribution function and variance influence adversely the quality of the assimilation approach. Variability of property distributions in the deep sea ranges typically comparable with the magnitude of observational errors bars. Uncertainties of space-based observations may be caused by errors related to cloud coverage or extraordinary aerosol loadings e.g. due to volcanic eruptions which can bias nighttime retrievals up to 2-4 °C (McClain et al., 1985).
- Residuals might also be related to the approximations for non-linear processes due to a limited integration time, a local minimum, weight of the penalty terms and/or the choice of the first guess.

7 Outlook

Future experiments will also be carried out with the adjoint HOPE-C model. Special emphasis could be placed on a systematic investigation of the sensitivity of the model's parameterisations (e.g., internal friction, parameterisation of deep water formation, choice of numerical scheme, model resolution, formulation of the boundary conditions) by identical twin experiments. These improved parameterisations could be used for future data assimilation experiments including already available data such as space-based observations (e.g. EUMETSAT <http://www.eumetsat.de/>, MODIS, <http://modis-ocean.gsfc.nasa.gov/>), reanalysis data from the National Center for Environmental Prediction (NCEP), and data of sea ice coverage into our assimilation scheme.

Efforts are made to develop a more detailed in situ observational monitoring system, which will cover large parts of the world ocean in the near future. The Tropical Atmosphere Ocean project (TAO) in the Equatorial Pacific (<http://www.pmel.noaa.gov/tao/>) is a successful example for such a continuous observing system. Other projects like the ARGO project (<http://www.noaa.gov>) with more than 3,000 observation buoys will deliver large data sets of temperature and salinity of the oceans. The computational efficiency of the adjoint C-HOPE would allow us to use these data and the historical database to simulate the long-term trend in the deep-sea circulation (Broecker, 1998).

Tasks in the far future would be coupling of the inverse model to other climate subsystems like the atmosphere (adjoint ECHO) and consideration of biogeochemical processes in the model (currently developed at the Max-Planck-Institute for Meteorology).

8 Visiting Scientists

Folgende Gastwissenschaftler nahmen an diesem Projekt teil. Sie wurden teilweise auch von EUMETSAT gefördert.

Prof. Arne Winguth

Department of Atmospheric and Oceanic Sciences
University of Wisconsin-Madison
1225 W. Dayton
Madison, WI53706

Besuchszeiten: 29.5.00 - 27.7.00; 15.5.01 - 20.7.01; 2.6.02 - 31.7.02.

Dr. Konstantin Beljaev

Laboratorio Nacional de Computacao Cientifica,
Petropolis
Brazil

Besuchszeiten: 1.8.01 - 31.8.01; 19.1.02 - 16.1.02.

9 Veröffentlichungen aus diesem Projekt

Tanjura, C. A. S, D. Müller, K. P. Belyaev, H. Haak, J. W. C. Sotil and *U. Cubasch*, 2002: A simulation of the 1997 El Nino and its correction with data assimilation and the TAO/TRITON data set. Relatorios de Pesquisa e Desenvolvimento No. 26/2002, Laboratorio Nacional de Computacao Cientifica, Petropolis, Brazil, ISSN 0101 6113, 35pp. submitted to JMSJ.

10 Literature

Barth, N., and C. Wunsch, Oceanographic experiment design by simulated annealing, *J. Phys. Oceanogr.*, 20, 1249-1263, 1990.

Belyaev, K., S. Meyers and J. O'Brien, Fokker-Planck equation application to data assimilation based on the Kalman-filter theory, *J. Math. Sci.* 99, 1393, 2000.

Belyaev, K., C. Tanajura and J. O'Brien, A data assimilation method used with an ocean circulation model and its application to the tropical Atlantic, *Appl. Math. Mod.* 25, 655-670, 2001.

- Broecker, W.S., Thermohaline Circulation, the Achilles Heel of Our Climate System: Will Man-Made CO₂ Upset the Current Balance?, *Science*, 278, 1582-1588, 1998.
- Drijfhout, S., Heinze, C., Latif, M., and Maier-Reimer, E., Mean Circulation and Internal Variability in an Ocean Primitive Equation Model, 26, 559-580, 1996.
- Fofonoff, N. P., and R. C. Millard Jr., Algorithms for computation of fundamental properties of seawater, *Unesco Techn. Pap. Mar. Sci.* 44, Unesco 1983.
- Gent, P. R., and J. C. McWilliams, Isopycnal mixing in models, *Journal of Phys. Oceanogr.* 20, 150-155, 1990.
- Ghil, M., and P. Malanotte-Rizzoli, Data Assimilation in Meteorology and Oceanography, *Adv. Geophys.*, 33, 141-266, 1991.
- Ghil, M., K. Ide, A. Bennett, P. Courtier, M. Kimoto, M. Nagata, M. Saiki and N. Sato, Data Assimilation in Meteorology and Oceanography, Universal Academy Press, Tokyo, 1997.
- Giering, R., Erstellung eines adjungierten Modells zur Assimilierung von Daten in ein Modell der globalen ozeanischen Zirkulation, Examensarbeit Nr. 44, Max-Planck-Inst. fuer Meteorol., Hamburg, Germany, 1996.
- Giering, R., and T. Kaminsky, Recipes for Adjoint Code Construction, Rep. 212, Max-Planck-Inst. fuer Meteorol., Hamburg, Germany, 1996.
- Giering, R., Tangent linear and adjoint models, in: *Inverse Methods in Global Biogeochemical Cycles*, AGU Geophysical Monograph Series, edited by P. Kasibhatla, M. Heimann, D. Harley, N. Mahowald, R. Prinn, and P. Rainer, 33-48, 2000.
- Gilbert, J. C., and C. Lemarechal, Some numerical experiments with variable storage quasi-Newton algorithms, *Mathematical Programming*, 45, 407-435, 1989.
- Gouretski, V., and K. Jancke, A new world ocean climatology: Objective analysis on neutral surfaces, WHP Special Analysis Center technical Report No. 3, Hamburg, Germany, 1998.
- Groetzner, A., Latif, M. and Barnett, P., A decadal climate cycle in the North Atlantic Ocean as simulated by the ECHO coupled GCM, *J. of Climate*, 11, 831-847, 1998.
- Hibler, W. D., A dynamic thermodynamic sea ice model, *J. of Phys. Oceanogr.*, 9, 815-846, 1979.
- Krueger, J., Simulated annealing: A tool for data assimilation into an almost steady model state, *J. Phys. Oceanogr.*, 23, 679-688, 1993.
- Latif, M., Stockdale, T., Wolff, J., Burgers, G., Maier-Reimer, E., Junge, M. M., Arpe, K., and Bengtsson, L., Climatology and variability in the ECHO coupled GCM. *Tellus, Ser. A*, 46, 351-366, 1994.
- Latif, M. and Barnett, T. P., Decadal climate variability over the North Pacific and North America: Dynamics and predictability, 9, 2407-2423, 1996.
- Legutke, S., and E. Maier-Reimer, Climatology of the HOPE-G global ocean general circulation model. Technical Report 21, German Climate Computer Center (DKRZ), Hamburg, Germany, 1999.
- Legutke, S., and R. Voss, The Hamburg Atmosphere-Ocean Coupled Circulation Model ECHO-G. Technical Report 18, German Climate Computer Center (DKRZ), Hamburg, Germany, 1999.
- Levitus, Sydney, United States, Climatological atlas of the world ocean. National Oceanic and Atmospheric Administration, Rockville, MD., NOAA Professional Paper 13, Dec., 1982. 173 pp., 1982.
- Levitus, S., T. Boyer, M. Conkright, T. O'Brien, J. Antonov, C. Stephens, L. Stathoplos, D. Johnson and R. Gelfeld, World Ocean Data Base (NODC, Washington, D.C.), 1998.

- Maier-Reimer, E., U. Mikolajewicz, and K. Hasselmann, 1993: Mean circulation of the Hamburg LSG OGCM and its sensitivity on the thermohaline surface forcing. *J. Phys. Oceanogr.*, 731-757, 1993.
- Malanotte-Rizzoli, P. (Ed.), *Modern Approaches to Data Assimilation in Ocean Modeling*, Elsevier, Amsterdam, 1996.
- Marotzke, J., R. Giering, Q. K. Zhang, D. Stainnier, C. N. Hill, and T. Lee, Construction of the adjoint MIT ocean general circulation model and application to Atlantic heat transport sensitivity, *J. Geophys. Research*, 104, 29529-29548, 1999.
- Marsland, S. J., J. Jungclaus, H. Haak, M. Latif, U. Mikolajewicz, and E. Maier-Reimer, C-HOPE: A global ocean/ice model with generalized curvilinear coordinates, in prep. (to be submitted to *J. Geophys. Res.*), 2002.
- McClain, P. E., W. G. Pichel, and C. C. Walto, Comparative Performance of AVHRR-Based Multichannel Sea Surface Temperatures, *J. Geophys. Research* 90, 11587-11601, 1985.
- Mikolajewicz, U., and E. Maier-Reimer, Mixed boundary conditions in ocean general circulation models and their influence on the stability of the model's conveyor belt. *J. Geophys. Res.* 99, C11, 22633-22644, 1994.
- Schiller, A., and J. Willebrand, A technique for the determination of surface heat and freshwater fluxes from hydrographic observations using an approximate adjoint ocean circulation model, *J. Mar. Res.*, 53, 433-451, 1995.
- Stammer, D., C. Wunsch, R. Giering, C. Eckert, P. Heimbach, J. Marotzke, A. Adcroft, C. N. Hill, and J. Marshall, The global ocean circulation and transport during 1992-1997, estimated from ocean observations and a general circulation model, Part 1: Methodology and estimated state, ECCO Report Series, Report 4, 2000.
- Stockdale, T., M. Latif, G. Burgers, and J.-O. Wolff, Some sensitivities of a coupled ocean-atmosphere GCM, *Tellus, Ser. A*, 46, 367-380, 1994.
- Stoessel, A., S.-J. Kim, and S. Drijfhout, The Impact of Southern Ocean Sea Ice in a Global Ocean Model, *J. of Phys. Oceanogr.*, 28, 1999-2018, 1998.
- Talagrand, O., The use of adjoint equations in numerical modeling of the atmospheric circulation, in: *Automatic Differentiation of Algorithms: Theory, Implementation and Application*, edited by A. Griewank and G. Corliss, 169-180, SIAM, Philadelphia, Penn., 1991.
- Tziperman, E., W. C. Thacker, R. B. Long, and S.-M. Hwang, Oceanic data analysis using a general circulation model: Part I Simulations, *J. Phys. Oceanogr.*, 22, 1434-1457, 1992.
- Venzke, S., M. Latif, and A. Villwock, The coupled GCM ECHO-2. Part II: Indian ocean response to ENSO, *J. of Climate*, 13, 1371-1383, 2000.
- Wenzel, M., J. Schroeter, and D. Olbers, The annual cycle of the global ocean circulation as determined by 4D VAR data, *Progress in Oceanography*, Vol. 48, Issue 1, 73-119, 2001.
- Winguth, A. M. E., Assimilation von ^{13}C -Daten aus marinen Sedimentbohrkernen in das LSG zur Rekonstruktion der Ozeanzirkulation waehrend des letzten glazialen Maximums, Examensarbeit Nr. 47, Max-Planck-Inst. fuer Meteorol., Hamburg, Germany, 1997.
- Winguth A. M. E., D. Archer, E. Maier-Reimer, and U. Mikolajewicz, Paleonutrient data analysis of the glacial Atlantic using an adjoint ocean general circulation model, Rep. 281, Max-Planck-Inst. fuer Meteorol., Hamburg, Germany, 1998.
- Winguth, A. M. E., D. Archer, J. C. Duplessy, E. Maier-Reimer, and U. Mikolajewicz, Sensitivity of paleonutrient tracer distributions and deep-sea circulation to glacial boundary conditions, *Paleoceanography*. 14(3), 304-323, 1999.
- Winguth, A. M. E., D. Archer, E. Maier-Reimer, and U. Mikolajewicz, Paleonutrient data analysis of the glacial Atlantic using an adjoint ocean general circulation model, in: *Inverse*

Methods in Global Biogeochemical Cycles, AGU Geophysical Monograph Series, edited by P. Kasibhatla, M. Heimann, D. Harley, N. Mahowald, R. Prinn, and P. Rainer, 171-183, 2000.
 Winguth, A. M. E., C. Heinze, J. E. Kutzbah, U. Mikolajewicz, D. Rowley, A. Rees, and A. M. Ziegler, Simulated warm polar currents during the Middle Permian Paleocyanography (in press), 2002.
 Wolff, J.-O., E. Maier-Reimer, and S. Legutke, The Hamburg Ocean Primitive Equation Model, Rep. 13, Deutsches Klimarechenzentrum, Hamburg, Germany, 1997.

11 Appendix A: Example of an Adjoint Program

Computer code from C-HOPE: subroutine RHOF1 (equation of state):

```

SUBROUTINE RHO1(T,S,P,RH)
#include "PARAM1.h"
C*****
C ZUSTANDSGLEICHUNG
C UNTERPROGRAMM NACH ADRIAN GILL (ANHANG)
C+++++
C
  DIMENSION S(IEJE),T(IEJE),RH(IEJE),S3H(IEJE)
  DATA B0,B1,B2,B3,B4/8.24493E-1,-4.0899E-3,7.6438E-5,
,-8.2467E-7,5.3875E-9/
  DATA C0,C1,C2/-5.72466E-3,1.0227E-4,-1.6546E-6/
  DATA D0/4.8314E-4/
  DATA A0,A1,A2,A3,A4,A5/999.842594,6.793952E-2,
,-9.095290E-3,1.001685E-4,-1.120083E-6,6.536332E-9/
  DATA F0,F1,F2,F3/54.6746,-0.603459,
,1.09987E-2,-6.1670E-5/
  DATA G0,G1,G2/7.944E-2,1.6483E-2,-5.3009E-4/
  DATA AI0,AI1,AI2/2.2838E-3,-1.0981E-5,-1.6078E-6/
  DATA AJ0/1.91075E-4/
  DATA AM0,AM1,AM2/-9.9348E-7,2.0816E-8,9.1697E-10/
  DATA E0,E1,E2,E3,E4/19652.21,148.4206,-2.327105,
,1.360477E-2,-5.155288E-5/
  DATA H0,H1,H2,H3/3.239908,1.43713E-3,
,1.16092E-4,-5.77905E-7/
  DATA AK0,AK1,AK2/8.50935E-5,-6.12293E-6,5.2787E-8/
C
  A0=999.8426
  F0=54.6746
  E0=19652.21
  E1=148.4206
  E2=-2.327105
  NH=IEJE
C
C

```

```

DO 100 N=1,NH
S(N)=MAX(S(N),28.)
S3H(N)=SQRT(S(N)**3)
100 CONTINUE

DO 200 N=1,NH
RH(N)=(A0+T(N)*(A1+T(N)
1 *(A2+T(N)*(A3+T(N)*(A4+T(N)*A5))))
1 +S(N)*(B0+T(N)*(B1+T(N)
1 *(B2+T(N)*(B3+T(N)*B4))))+D0*S(N)**2
++S3H(N)*(C0+T(N)*(C1+C2*T(N))) )
1 /(1.-P/(P*(
1 H0+T(N)*(H1+T(N)*(H2+T(N)*H3))
1 +S(N)*(AI0+T(N)*(AI1+AI2*T(N)))+AJ0*S3H(N)
1 +(AK0+T(N)*(AK1+T(N)*AK2)
1 +S(N)*(AM0+T(N)*(AM1+T(N)*AM2)))*P)+
1 E0+T(N)*(E1+T(N)*(E2+T(N)*(E3+T(N)*E4)))
1 +S(N)*(F0+T(N)*(F1+T(N)*(F2+T(N)*F3)))
1 +S3H(N)*(G0+T(N)*(G1+G2*T(N))))))
200 CONTINUE
RETURN
END

```

Adjoint computer code from C-HOPE: subroutine ADRHOF1

```

subroutine adrhof1( t, s, p, adt, ads, adp, adrh )
#include "PARAM1.h"
C*****
C ADJOINT BY A. WINGUTH 06/2001
C ZUSTANDSGLEICHUNG
C UNTERPROGRAMM NACH ADRIAN GILL (ANHANG)
C
C** Tangent linear and Adjoint Model Compiler, TAMC 5.3.0 **
C*****
C=====
C define arguments
C=====
    real adrh(ieje)
    real ads(ieje)
    real adt(ieje)
    real s(ieje)
    real t(ieje)

C=====
C define local variables
C=====

```

```
real ads3h(ieje)
real s3h(ieje)
real sh(ieje)
```

```
C=====
C define data
C=====
data b0,b1,b2,b3,b4/8.24493e-1,-4.0899e-3,7.6438e-5,-8.2467e-7,
$5.3875e-9/
data c0,c1,c2/-5.72466e-3,1.0227e-4,-1.6546e-6/
data d0/4.8314e-4/
data a0,a1,a2,a3,a4,a5/999.842594,6.793952e-2,-9.095290e-3,
$1.001685e-4,-1.120083e-6,6.536332e-9/
data f0,f1,f2,f3/54.6746,-0.603459,1.09987e-2,-6.1670e-5/
data g0,g1,g2/7.944e-2,1.6483e-2,-5.3009e-4/
data ai0,ai1,ai2/2.2838e-3,-1.0981e-5,-1.6078e-6/
data aj0/1.91075e-4/
data am0,am1,am2/-9.9348e-7,2.0816e-8,9.1697e-10/
data e0,e1,e2,e3,e4/19652.21,148.4206,-2.327105,1.360477e-2,-
$5.155288e-5/
data h0,h1,h2,h3/3.239908,1.43713e-3,1.16092e-4,-5.77905e-7/
data ak0,ak1,ak2/8.50935e-5,-6.12293e-6,5.2787e-8/
```

```
C-----
C SAVE ARGUMENTS
C-----
do ip1 = 1, ieje
sh(ip1) = s(ip1)
end do
```

```
C-----
C RESET LOCAL ADJOINT VARIABLES
C-----
do ip1 = 1, ieje
ads3h(ip1) = 0.
end do
```

```
C-----
C ROUTINE BODY
C-----
a0 = 999.8426
f0 = 54.6746
e0 = 19652.21
e1 = 148.4206
e2 = -2.327105
nh = ieje
do n = 1, nh
```

```

s(n) = max(s(n),28.)
s3h(n) = sqrt(s(n)**3)
end do
do n = 1, nh
  adp = adp+adrh(n)*((a0+t(n)*(a1+t(n)*(a2+t(n)*(a3+t(n)*(a4+t(n)*
$a5))))+s(n)*(b0+t(n)*(b1+t(n)*(b2+t(n)*(b3+t(n)*b4)))))+d0*s(n)**2+
$s3h(n)*(c0+t(n)*(c1+c2*t(n))))*(1/(p*(h0+t(n)*(h1+t(n)*(h2+t(n)*
$h3)))+s(n)*(ai0+t(n)*(ai1+ai2*t(n))))+aj0*s3h(n)+(ak0+t(n)*(ak1+t(n)
*$ak2)+s(n)*(am0+t(n)*(am1+t(n)*am2))))*p)+e0+t(n)*(e1+t(n)*(e2+t(n)
*(e3+t(n)*e4)))+s(n)*(f0+t(n)*(f1+t(n)*(f2+t(n)*f3)))+s3h(n)*(g0+
$t(n)*(g1+g2*t(n))))-p*(p*(ak0+t(n)*(ak1+t(n)*ak2)+s(n)*(am0+t(n)*
$(am1+t(n)*am2))))+h0+t(n)*(h1+t(n)*(h2+t(n)*h3))+s(n)*(ai0+t(n)*
$(ai1+ai2*t(n))))+aj0*s3h(n)+(ak0+t(n)*(ak1+t(n)*ak2)+s(n)*(am0+t(n)
*(am1+t(n)*am2))))*p)/((p*(h0+t(n)*(h1+t(n)*(h2+t(n)*h3)))+s(n)*
$(ai0+t(n)*(ai1+ai2*t(n))))+aj0*s3h(n)+(ak0+t(n)*(ak1+t(n)*ak2)+s(n)
*(am0+t(n)*(am1+t(n)*am2))))*p)+e0+t(n)*(e1+t(n)*(e2+t(n)*(e3+t(n)*
$e4)))+s(n)*(f0+t(n)*(f1+t(n)*(f2+t(n)*f3)))+s3h(n)*(g0+t(n)*(g1+
$g2*t(n))))*(p*(h0+t(n)*(h1+t(n)*(h2+t(n)*h3)))+s(n)*(ai0+t(n)*(ai1+
$ai2*t(n))))+aj0*s3h(n)+(ak0+t(n)*(ak1+t(n)*ak2)+s(n)*(am0+t(n)*
$(am1+t(n)*am2))))*p)+e0+t(n)*(e1+t(n)*(e2+t(n)*(e3+t(n)*e4)))+s(n)*
$(f0+t(n)*(f1+t(n)*(f2+t(n)*f3)))+s3h(n)*(g0+t(n)*(g1+g2*t(n)))))/
$((1.-p/(p*(h0+t(n)*(h1+t(n)*(h2+t(n)*h3)))+s(n)*(ai0+t(n)*(ai1+ai2*
$t(n))))+aj0*s3h(n)+(ak0+t(n)*(ak1+t(n)*ak2)+s(n)*(am0+t(n)*(am1+
$t(n)*am2))))*p)+e0+t(n)*(e1+t(n)*(e2+t(n)*(e3+t(n)*e4)))+s(n)*(f0+
$t(n)*(f1+t(n)*(f2+t(n)*f3)))+s3h(n)*(g0+t(n)*(g1+g2*t(n))))*(1.-
$p/(p*(h0+t(n)*(h1+t(n)*(h2+t(n)*h3)))+s(n)*(ai0+t(n)*(ai1+ai2*t(n)
)$)+aj0*s3h(n)+(ak0+t(n)*(ak1+t(n)*ak2)+s(n)*(am0+t(n)*(am1+t(n)*
$am2))))*p)+e0+t(n)*(e1+t(n)*(e2+t(n)*(e3+t(n)*e4)))+s(n)*(f0+t(n)*
$(f1+t(n)*(f2+t(n)*f3)))+s3h(n)*(g0+t(n)*(g1+g2*t(n))))))
  ads(n) = ads(n)+adrh(n)*((b0+t(n)*(b1+t(n)*(b2+t(n)*(b3+t(n)*b4)
$))+2*d0*s(n))/(1.-p/(p*(h0+t(n)*(h1+t(n)*(h2+t(n)*h3)))+s(n)*(ai0+
$t(n)*(ai1+ai2*t(n))))+aj0*s3h(n)+(ak0+t(n)*(ak1+t(n)*ak2)+s(n)*
$(am0+t(n)*(am1+t(n)*am2))))*p)+e0+t(n)*(e1+t(n)*(e2+t(n)*(e3+t(n)*
$e4)))+s(n)*(f0+t(n)*(f1+t(n)*(f2+t(n)*f3)))+s3h(n)*(g0+t(n)*(g1+
$g2*t(n)))))-(a0+t(n)*(a1+t(n)*(a2+t(n)*(a3+t(n)*(a4+t(n)*a5))))+
$s(n)*(b0+t(n)*(b1+t(n)*(b2+t(n)*(b3+t(n)*b4)))))+d0*s(n)**2+s3h(n)*
$(c0+t(n)*(c1+c2*t(n))))*(p*(p*(ai0+t(n)*(ai1+ai2*t(n)))+(am0+t(n)*
$(am1+t(n)*am2))))*p)+f0+t(n)*(f1+t(n)*(f2+t(n)*f3)))/((p*(h0+t(n)*
$(h1+t(n)*(h2+t(n)*h3)))+s(n)*(ai0+t(n)*(ai1+ai2*t(n))))+aj0*s3h(n)+
$(ak0+t(n)*(ak1+t(n)*ak2)+s(n)*(am0+t(n)*(am1+t(n)*am2))))*p)+e0+
$t(n)*(e1+t(n)*(e2+t(n)*(e3+t(n)*e4)))+s(n)*(f0+t(n)*(f1+t(n)*(f2+
$t(n)*f3)))+s3h(n)*(g0+t(n)*(g1+g2*t(n))))*(p*(h0+t(n)*(h1+t(n)*
$(h2+t(n)*h3)))+s(n)*(ai0+t(n)*(ai1+ai2*t(n))))+aj0*s3h(n)+(ak0+t(n)*
$(ak1+t(n)*ak2)+s(n)*(am0+t(n)*(am1+t(n)*am2))))*p)+e0+t(n)*(e1+t(n)
*(e2+t(n)*(e3+t(n)*e4)))+s(n)*(f0+t(n)*(f1+t(n)*(f2+t(n)*f3)))+
$s3h(n)*(g0+t(n)*(g1+g2*t(n)))))/((1.-p/(p*(h0+t(n)*(h1+t(n)*(h2+
$t(n)*h3)))+s(n)*(ai0+t(n)*(ai1+ai2*t(n))))+aj0*s3h(n)+(ak0+t(n)*

```

$$\begin{aligned}
& \$(ak1+t(n)*ak2)+s(n)*(am0+t(n)*(am1+t(n)*am2)))^p)+e0+t(n)*(e1+t(n) \\
& \$(e2+t(n)*(e3+t(n)*e4)))+s(n)*(f0+t(n)*(f1+t(n)*(f2+t(n)*f3)))+ \\
& \$(s3h(n)*(g0+t(n)*(g1+g2*t(n))))*(1.-p/(p*(h0+t(n)*(h1+t(n)*(h2+ \\
& \$(t(n)*h3)))+s(n)*(ai0+t(n)*(ai1+ai2*t(n)))+aj0*s3h(n)+(ak0+t(n)* \\
& \$(ak1+t(n)*ak2)+s(n)*(am0+t(n)*(am1+t(n)*am2)))^p)+e0+t(n)*(e1+t(n) \\
& \$(e2+t(n)*(e3+t(n)*e4)))+s(n)*(f0+t(n)*(f1+t(n)*(f2+t(n)*f3)))+ \\
& \$(s3h(n)*(g0+t(n)*(g1+g2*t(n))))))
\end{aligned}$$

$$\begin{aligned}
& ads3h(n) = ads3h(n)+adrh(n)*((c0+t(n)*(c1+c2*t(n)))/(1.-p/(p* \\
& \$(h0+t(n)*(h1+t(n)*(h2+t(n)*h3)))+s(n)*(ai0+t(n)*(ai1+ai2*t(n)))+ \\
& \$(aj0*s3h(n)+(ak0+t(n)*(ak1+t(n)*ak2)+s(n)*(am0+t(n)*(am1+t(n)*am2) \\
& \$(s)*p)+e0+t(n)*(e1+t(n)*(e2+t(n)*(e3+t(n)*e4)))+s(n)*(f0+t(n)*(f1+ \\
& \$(t(n)*(f2+t(n)*f3)))+s3h(n)*(g0+t(n)*(g1+g2*t(n)))))-(a0+t(n)*(a1+ \\
& \$(t(n)*(a2+t(n)*(a3+t(n)*(a4+t(n)*a5)))))+s(n)*(b0+t(n)*(b1+t(n)*(b2+ \\
& \$(t(n)*(b3+t(n)*b4)))))+d0*s(n)**2+s3h(n)*(c0+t(n)*(c1+c2*t(n))))*(p* \\
& \$(p*aj0+g0+t(n)*(g1+g2*t(n)))/(p*(h0+t(n)*(h1+t(n)*(h2+t(n)*h3)))+ \\
& \$(s(n)*(ai0+t(n)*(ai1+ai2*t(n)))+aj0*s3h(n)+(ak0+t(n)*(ak1+t(n)*ak2) \\
& \$(s)+s(n)*(am0+t(n)*(am1+t(n)*am2)))^p)+e0+t(n)*(e1+t(n)*(e2+t(n)*(e3+ \\
& \$(t(n)*e4)))+s(n)*(f0+t(n)*(f1+t(n)*(f2+t(n)*f3)))+s3h(n)*(g0+t(n)* \\
& \$(g1+g2*t(n))))*(p*(h0+t(n)*(h1+t(n)*(h2+t(n)*h3)))+s(n)*(ai0+t(n)* \\
& \$(ai1+ai2*t(n)))+aj0*s3h(n)+(ak0+t(n)*(ak1+t(n)*ak2)+s(n)*(am0+t(n) \\
& \$(s)*(am1+t(n)*am2)))^p)+e0+t(n)*(e1+t(n)*(e2+t(n)*(e3+t(n)*e4)))+s(n) \\
& \$(s)*(f0+t(n)*(f1+t(n)*(f2+t(n)*f3)))+s3h(n)*(g0+t(n)*(g1+g2*t(n)))))) \\
& \$(/((1.-p/(p*(h0+t(n)*(h1+t(n)*(h2+t(n)*h3)))+s(n)*(ai0+t(n)*(ai1+ \\
& \$(ai2*t(n)))+aj0*s3h(n)+(ak0+t(n)*(ak1+t(n)*ak2)+s(n)*(am0+t(n)* \\
& \$(s)*(am1+t(n)*am2)))^p)+e0+t(n)*(e1+t(n)*(e2+t(n)*(e3+t(n)*e4)))+s(n)* \\
& \$(s)*(f0+t(n)*(f1+t(n)*(f2+t(n)*f3)))+s3h(n)*(g0+t(n)*(g1+g2*t(n))))))
\end{aligned}$$

$$\begin{aligned}
& adt(n) = adt(n)+adrh(n)*((t(n)*(t(n)*(t(n)*(t(n)*a5+a4+t(n)*a5)+ \\
& \$(a3+t(n)*(a4+t(n)*a5))+a2+t(n)*(a3+t(n)*(a4+t(n)*a5)))+a1+t(n)*(a2+ \\
& \$(t(n)*(a3+t(n)*(a4+t(n)*a5)))+s(n)*(t(n)*(t(n)*(t(n)*b4+b3+t(n)*b4) \\
& \$(+b2+t(n)*(b3+t(n)*b4))+b1+t(n)*(b2+t(n)*(b3+t(n)*b4)))+s3h(n)* \\
& \$(t(n)*c2+c1+c2*t(n)))/(1.-p/(p*(h0+t(n)*(h1+t(n)*(h2+t(n)*h3)))+ \\
& \$(s(n)*(ai0+t(n)*(ai1+ai2*t(n)))+aj0*s3h(n)+(ak0+t(n)*(ak1+t(n)*ak2) \\
& \$(s)+s(n)*(am0+t(n)*(am1+t(n)*am2)))^p)+e0+t(n)*(e1+t(n)*(e2+t(n)*(e3+ \\
& \$(t(n)*e4)))+s(n)*(f0+t(n)*(f1+t(n)*(f2+t(n)*f3)))+s3h(n)*(g0+t(n)* \\
& \$(g1+g2*t(n))))-(a0+t(n)*(a1+t(n)*(a2+t(n)*(a3+t(n)*(a4+t(n)*a5)))) \\
& \$(s)+s(n)*(b0+t(n)*(b1+t(n)*(b2+t(n)*(b3+t(n)*b4)))))+d0*s(n)**2+ \\
& \$(s3h(n)*(c0+t(n)*(c1+c2*t(n))))*(p*(p*(t(n)*(t(n)*h3+h2+t(n)*h3)+ \\
& \$(h1+t(n)*(h2+t(n)*h3)+s(n)*(t(n)*ai2+ai1+ai2*t(n)))+(t(n)*ak2+ak1+ \\
& \$(t(n)*ak2+s(n)*(t(n)*am2+am1+t(n)*am2))^p)+t(n)*(t(n)*(t(n)*e4+e3+ \\
& \$(t(n)*e4)+e2+t(n)*(e3+t(n)*e4))+e1+t(n)*(e2+t(n)*(e3+t(n)*e4)))+s(n) \\
& \$(s)*(t(n)*(t(n)*f3+f2+t(n)*f3)+f1+t(n)*(f2+t(n)*f3))+s3h(n)*(t(n)*g2+ \\
& \$(g1+g2*t(n)))/(p*(h0+t(n)*(h1+t(n)*(h2+t(n)*h3)))+s(n)*(ai0+t(n)* \\
& \$(s)*(ai1+ai2*t(n)))+aj0*s3h(n)+(ak0+t(n)*(ak1+t(n)*ak2)+s(n)*(am0+t(n)
\end{aligned}$$

```

$(am1+t(n)*am2))*p)+e0+t(n)*(e1+t(n)*(e2+t(n)*(e3+t(n)*e4)))+s(n)
$(f0+t(n)*(f1+t(n)*(f2+t(n)*f3)))+s3h(n)*(g0+t(n)*(g1+g2*t(n))))*
$(p*(h0+t(n)*(h1+t(n)*(h2+t(n)*h3)))+s(n)*(ai0+t(n)*(ai1+ai2*t(n)))+
$aj0*s3h(n)+(ak0+t(n)*(ak1+t(n)*ak2)+s(n)*(am0+t(n)*(am1+t(n)*am2))
$)*p)+e0+t(n)*(e1+t(n)*(e2+t(n)*(e3+t(n)*e4)))+s(n)*(f0+t(n)*(f1+
$(t(n)*(f2+t(n)*f3)))+s3h(n)*(g0+t(n)*(g1+g2*t(n)))))/((1.-p/(p*
$(h0+t(n)*(h1+t(n)*(h2+t(n)*h3)))+s(n)*(ai0+t(n)*(ai1+ai2*t(n)))+
$aj0*s3h(n)+(ak0+t(n)*(ak1+t(n)*ak2)+s(n)*(am0+t(n)*(am1+t(n)*am2))
$)*p)+e0+t(n)*(e1+t(n)*(e2+t(n)*(e3+t(n)*e4)))+s(n)*(f0+t(n)*(f1+
$(t(n)*(f2+t(n)*f3)))+s3h(n)*(g0+t(n)*(g1+g2*t(n))))*(1.-p/(p*(h0+
$(t(n)*(h1+t(n)*(h2+t(n)*h3)))+s(n)*(ai0+t(n)*(ai1+ai2*t(n)))+aj0*
$)s3h(n)+(ak0+t(n)*(ak1+t(n)*ak2)+s(n)*(am0+t(n)*(am1+t(n)*am2)))*p)
$+e0+t(n)*(e1+t(n)*(e2+t(n)*(e3+t(n)*e4)))+s(n)*(f0+t(n)*(f1+t(n)*
$(f2+t(n)*f3)))+s3h(n)*(g0+t(n)*(g1+g2*t(n))))))
    adrh(n) = 0.
end do
do ip1 = 1, ieje
    s(ip1) = sh(ip1)
end do
do n = 1, nh
    s(n) = max(s(n),28.)
    ads(n) = ads(n)+3*ads3h(n)*1./(2.*sqrt(s(n)**3))*s(n)**2
    ads3h(n) = 0.
    do ip1 = 1, ieje
        s(ip1) = sh(ip1)
    end do
    ads(n) = ads(n)*(0.5+sign(0.5,s(n)-28.))
end do

end

```

12 Appendix B: Algorithm for Testing Cost Gradient Produced by the Adjoint Code

The cost gradient produced by the adjoint code can be tested by a Taylor series expansion. The gradient of the cost function can be in first order finite difference

$$\frac{dJ_r}{dy} \approx \frac{\Delta J}{\Delta y} \quad (17)$$

Here we use the testing algorithm developed by Long (pers. comm.):

1. Run a control simulation R_0 with unperturbed control variables \bar{y}_0 to produce a set of "observations".

2. Generate a first guess by perturbation of the control variables $\bar{y}_r = 1.1 \bar{y}_0$ and calculation of the norm of $\|\bar{y}_r\| = \sqrt{\Sigma y_r^2}$. This defines the reference state at which the directional gradient will be computed, first with the adjoint then by finite differences.
3. Run the model with the reference initial conditions to get the reference cost J_r .
4. Run the adjoint model to get the reference gradient vector ∇J_r by "backward" integration of the adjoint model. Computation of the component in direction of \bar{y}_r :

$$\frac{dJ_r}{dy} = \frac{\bar{y}_r \nabla J_r}{\|\bar{y}_r\|_2}$$

(18)

5. Perturbation of the control variables $\bar{y}_i = a_i \bar{y}_r$, with $a_i = 1 + 10^{-(2+i)}$, $i = 1, \dots, n$. The index i denotes the i -th perturbation of the reference state and the perturbation factor b_i is a number slightly larger than 1 (e.g. 1.001 for $i=1$). The size of the perturbation is $\Delta y_i = \|\bar{y}_i\|_2 - \|\bar{y}_r\|_2 = (a_i - 1) \|\bar{y}_r\|_2$.

6. Run the model to get the corresponding value of the cost J_i

$$\left(\frac{\Delta J}{\Delta y}\right)_i = \frac{J_i - J_r}{(a_i - 1) \|\bar{y}_r\|_2} \quad (19)$$

7. The ratio of $\left(\frac{\Delta J}{\Delta y}\right)_i / \left(\frac{dJ_r}{dy}\right)$ should be 1 if truncation errors are neglected. Including truncation error, the ratio should converge linearly to 1 as dx gets very small until round-off error becomes a problem.

Berichtsblatt

1 ISBN oder ISSN siehe Anlage	2 Berichtsart Abschlussbericht
3a Titel des Berichts PRAOMS: Entwicklung eines prä-operationellen Assimilationssystem für Ozean- und Meereisfelder aus Satelliten- daten	
3b Titel der Publikation siehe Anlage	
4a Autoren des Berichts (Name, Vorname(n)) Cubasch, Dr. Ulrich Müller, Dr. Detlev	5. Abschlußdatum des Vorhabens 31.12.2001
4b Autoren der Publikation (Name, Vorname(n)) siehe Anlage	6. Veröffentlichungsdatum siehe Anlage
	7 Form der Publikation siehe Anlage
8. Durchführende Institution(en) (Name, Adresse) Max-Planck-Institut für Meteorologie Bundesstrasse 55 20146 Hamburg	9. Ber. Nr. Durchführende Institution /
	10 Förderkennzeichen *) 07DLR09(S)D 1
	11a. Seitenzahl Bericht 49
	11b. Seitenzahl Publikation siehe Anlage
13. Fördernde Institution (Name, Adresse) Bundesministerium für Bildung und Forschung (BMBF) 53170 Bonn	12 Literaturangaben 42
	14. Tabellen 0
	15. Abbildungen 21
16 Zusätzliche Angaben	
17. Vorgelegt bei (Titel, Ort, Datum) SAF Training Workshop, Ocean and Sea-Ice, Perros-Guiree, FR, 30. Nov. bis 02. Dez. 1999 SAF Training Workshop, Climate Monitoring, Dresden, DE, 20. bis 22 Nov. 2000	
18 Kurzfassung siehe Anlage	
19 Schlagwörter siehe Anlage	
20 Verlag siehe Anlage	21 Preis /

*) Auf das Förderkennzeichen des BMBF soll auch in der Veröffentlichung hingewiesen werden

Anlage zum Berichtsblatt

zu Punkt 3b (schliesst ein: Punkt 4b Autoren, 7 Form, 11b Seitenzahl, 20 Verlag)

Berichte

Cyclostationary Circulation Estimation with a Global Assimilation System

D. Müller, R. Giering, U. Mikolajewicz, E. Maier-Reimer, 1998

MPIMET Report 279, Hamburg, 32 pp

http://www.mpimet.mpg.de/de/web/science/a_reports_archive.php?actual=1998

A Kalman Filter for Ocean Monitoring

K. Belyaev, D. Müller, 2002

<http://arxiv.org/abs/physics/0207097>, 16 pp

begutachtete Literatur

D. Müller, 1999: Ocean State Estimation for Climate Monitoring

SAF Trainings Workshop Ocean and Sea Ice, Eumetsat EUMP27, 89 – 104, 15 pages

http://www.eumetsat.de/en/area2/conf_proceeds.html

D. Müller, U. Cubasch, K. Koltermann, P. Loewe, 2000: Ocean Data Assimilation for Climate Monitoring, SAF Trainings Workshop Climate Monitoring,

Eumetsat EUMP31, 110-119, 10 pages,

http://www.eumetsat.de/en/area2/conf_proceeds.html

K. Belyaev, H. Haak, U. Cubasch, D. Müller, 2002: A Kalman Filter for Ocean Monitoring,

http://www.eumetsat.de/en/area4/saf/internet/vs/vs_reports/vs_reports.html, 23 pages

K. Belyaev, C. Tanajura, D. Müller, U. Cubasch, 2002

A Data assimilation Method and its Application to the HOPE Model

Simulation of the 1997 El Nino

Proc. of the 12th Congresso do Socio da Meteorologia Brasileiro,

Foz-de-Iguassu, Brazil, 4-9 August 2002

A Simulation of the 1997 El Nino and its Correction with Data Assimilation and the TAO/TRITON data set.

Tanajura, C. A. S, D. Müller, K. P Belyaev, H. Haak, J. W. C. Sotil and U. Cubasch, 2002,

Relatorios de Pesquisa e Desenvolvimento No. 26/2002, Laboratorio Nacional de

Computacao Cientifica, Petropolis, Brazil, ISSN 0101 6113, 35 pp. submitted to JMSJ.

<http://www.lncc.br/proj-pesq/rpesq.html>

zu Punkt 18

Kurzfassung

Neuartige Beobachtungstechniken liefern einen im Wesentlichen kontinuierlichen Strom von Ozean Daten mit bisher unbekanntem Detailreichtum. Die wissenschaftliche und operationelle Ausbeutung dieser Daten erfordert ihre enge Einbindung in numerische Modelle der globalen Ozean Zirkulation. Diese Modelle schaffen die

Grundlagen für: Simulation/Assimilation und schließlich Verständnis der Beobachtungen, dynamische Extrapolation der Daten in der Raum-Zeit und im Phasenraum, Qualitätssicherung von Modellen und Daten, Reduktion der Beobachtungskosten. Diese Modell-Daten Kombination eröffnet weite, neue Felder für Klima Monitoring, Ozeanographie und Marine Industrie wie Schifffahrt, Fischerei, Küstenindustrie usw.

PRAOMS hat Software Pakete zur Simulation, Assimilation und zum Daten Management in der globalen Ozean Zustandsschätzung getestet und eingesetzt. Als Modell Komponenten wurden das Hamburg LSG Modell und die GROB Version des Hamburg Ocean Primitive Equation Model HOPE für die Schätzung betrachtet. Das LSG Modell ist den speziellen Anforderungen der globalen Langzeitintegrationen in der Biogeochemie und der Paleoceanographie angepasst, während das HOPE Modell mit seinen hochauflösenden Regionen sogar das Studium von mesoskaligen Prozessen erlaubt.

Die adjungierte Variationsmethode und der sequentielle Kalman Filter sind die fortgeschrittensten Assimilationsverfahren. Beide Ansätze wurden erfolgreich getestet und angewandt. Für das LSG Modell wurde der adjungierte Code entwickelt und implementiert. Die LSG Adjungierte wurde zur Assimilation von Dichtedaten des World Ocean Atlas benutzt. Die Assimilation lieferte eine signifikant verbesserte Schätzung der Wassermassen Verteilung, speziell im tiefen Ozean. Für GROB HOPE wurde die Fokker-Planck Darstellung des Kalman Filters entwickelt. Dieser Zustandsschätzer wurde auf die Assimilation täglicher Ozean Oberflächen Temperaturen sowie monatlicher Temperaturen des Ozeaninneren vom TAO/TRITON Netzwerk im Äquatorialen Pazifik für das El Nino Jahr 1997 angewandt. Die Modell-Daten Kombination verbessert wesentlich die Darstellung der für El Nino charakteristischen ozeanischen Transportprozesse, wie Wellenausbreitung, Mischen und Up- und Downwelling. Beiträge numerisch induzierter Diffusion wurden auf ein realistisches Mass reduziert. Die Schätzung liefert die Basis für praktisch relevante Kurzzeit Klimavorhersagen.

zu Punkt 19 *Schlagwörter*

Ocean state estimation, Hamburg LSG Model, HOPE Model
Variational assimilation, cost function, adjoint model, adjoint code compiler
Sequential assimilation, Kalman Filter, stochastic process, Fokker-Planck Equation

Document Control Sheet

1. ISBN or ISSN attached	2. Type of Report final report
3a. Report Title PRAOMS: Development of a pre-operational assimilationssystem for ocean- and sea-ice-fields from satellite data	
3b. Title of Publication attached	
4a. Author(s) of the Report (Family Name, First Name(s)) Cubasch, Dr. Ulrich Müller, Dr. Detlev	5. End of Project 31.12.2001
4b. Author(s) of the Publication (Family Name, First Name(s)) attached	6. Publication Date attached
8. Performing Organization(s) (Name, Address) Max-Planck-Institut für Meteorologie Bundesstrasse 55 20146 Hamburg	7. Form of Publication attached
13. Sponsoring Agency (Name, Address) Bundesministerium für Bildung und Forschung (BMBF) 53170 Bonn	9. Originator's Report No /
16. Supplementary Notes	10. Reference No. 07DLR09(8)D1
17. Presented at (Title, Place, Date) SAF Training Workshop, Ocean and Sea-Ice, Perros-Guiree, FR, 30. Nov. bis 02. Dec. 1999 SAF Training Workshop, Climate Monitoring, Dresden, DE, 20. bis 22 Nov. 2000	11a. No. of Pages Report 49
18. Abstract attached	11b. No. of Pages Publication attached
19. Keywords attached	12. No. of References 42
20. Publisher attached	14. No. of Tables 0
21. Price /	15. No. of Figures 21

Document Control Sheet (Attachment)

Top 3b (enclosed: 4b Authors, 7 Form, 11b No. of pages , 20 Publisher)

Reports

Cyclostationary Circulation Estimation with a Global Assimilation System

D. Müller, R. Giering, U. Mikolajewicz, E. Maier-Reimer, 1998

MPIMET Report 279, Hamburg, 32 pp

http://www.mpimet.mpg.de/de/web/science/a_reports_archive.php?actual=1998

A Kalman Filter for Ocean Monitoring

K. Belyaev, D. Müller, 2002

<http://arxiv.org/abs/physics/0207097>, 16 pp

Refereed Literature

D. Müller, 1999: Ocean State Estimation for Climate Monitoring

SAF Trainings Workshop Ocean and Sea Ice, Eumetsat EUMP27, 89 – 104, 15 pages

http://www.eumetsat.de/en/area2/conf_proceeds.html

D. Müller, U. Cubasch, K. Koltermann, P. Loewe, 2000: Ocean Data Assimilation for Climate Monitoring, SAF Trainings Workshop Climate Monitoring,

Eumetsat EUMP31, 110-119, 10 pages

http://www.eumetsat.de/en/area2/conf_proceeds.html

K. Belyaev, H. Haak, U. Cubasch, D. Müller, 2002: A Kalman Filter for Ocean Monitoring,

http://www.eumetsat.de/en/area4/saf/internet/vs/vs_reports/vs_reports.html, 23 pages

K. Belyaev, C. Tanajura, D. Müller, U. Cubasch, 2002

A Data assimilation Method and its Application to the HOPE Model

Simulation of the 1997 El Nino

Proc. of the 12th Congresso do Socio da Meteorologia Brasileiro,

Foz-de-Iguassu, Brazil, 4-9 August 2002

A Simulation of the 1997 El Nino and its Correction with Data Assimilation and the TAO/TRITON data set.

Tanajura, C. A. S, D. Müller, K. P Belyaev, H. Haak, J. W. C. Sotil and U. Cubasch, 2002,

Relatorios de Pesquisa e Desenvolvimento No. 26/2002, Laboratorio Nacional de

Computacao Cientifica, Petropolis, Brazil, ISSN 0101 6113, 35 pp. submitted to JMSJ.

<http://www.lncc.br/proj-pesq/rpesq.html>

Top 18

Abstract

Novel observation techniques provide an essentially continuous stream of ocean data of previously unknown detail. Scientific and operational exploitation of this wealth requires a close linkage with numerical models of the global ocean circulation. Such models yield the foundations for: simulation/assimilation and ultimately understanding of the observational record, dynamical extrapolation of

data in space-time and phase space, quality assessment of models and data, reducing observational expenditure. This model-data combination opens wide and new fields for climate monitoring, oceanography and marine industries such as shipping, fisheries, coastal industry etc.

PRAOMS tested and established software packages in simulation, assimilation and data management for global ocean state estimation. As model components, the Hamburg LSG Model and the GROB version of the Hamburg Ocean Primitive Equation Model HOPE were considered for estimation. The LSG Model is tailored to the needs of global long-term integrations in biogeochemistry and paleoceanography, while the HOPE Model with its high-resolution regions allows even the study of mesoscale dynamics.

Advanced assimilation algorithms come as variational Adjoint Method and as sequential Kalman Filter. Both approaches were successfully tested and applied. For the LSG Model, the adjoint code was developed and implemented. The LSG Adjoint was used to assimilate buoyancy data of the World Ocean Atlas resulting in a significant improvement of the representation of the water mass distribution, particularly in the abyssal ocean. For GROB HOPE, the Fokker-Planck representation of the Kalman Filter was developed. This estimator was applied to the assimilation of daily global sea-surface temperatures together with monthly subsurface temperatures from the TAO/TRITON array in the equatorial Pacific for the El Nino year 1997. The model-data combination significantly improves the representation of oceanic transport processes associated with El Nino such as wave propagation, mixing and up- and down-welling. The role of numerically induced diffusion is reduced to a realistic measure. The estimate provides the basis for practically relevant short-term climate predictions.

Top 19

Keywords

Ocean state estimation, Hamburg LSG Model, HOPE Model
Variational assimilation, cost function, adjoint model, adjoint code compiler
Sequential assimilation, Kalman Filter, stochastic process, Fokker-Planck Equation